bioRxiv preprint doi: https://doi.org/10.1101/2024.08.13.607559; this version posted August 13, 2024. The copyright holder for this preprint (which was not certified by peer review) is the author/funder, who has granted bioRxiv a license to display the preprint in perpetuity. It is made available under aCC-BY-NC-ND 4.0 International license.

A cleaved cytosolic FOXG1 promotes excitatory neurogenesis by modulation of mitochondrial translation – a new therapeutic target for brain disorders.

Hannah Bruce,[1,2], Marnie E. Halpern[4], Clinton Monfries[2], Oniz Suleyman[2], Fursham Hamid[2], & Corinne Houart[1,2,3].

Corresponding authors: Hannah Bruce; hannah.1.bruce@kcl.ac.uk; Corinne Houart; corinne.houart@kcl.ac.uk

Affiliations:

(1) MRC Centre for Neurodevelopmental Disorders, Institute of Psychiatry, Psychology & Neuroscience, King's College London, London, SE1 1UL.
(2) Centre for Developmental Neurobiology, Institute of Psychiatry, Psychology & Neuroscience, King's College London, London, SE1 1UL.
(3) Francis Crick Institute, Midland Road, London, NW1 1AT.
(4) Geisel School of Medicine, Molecular and Systems Biology, Dartmouth, Hanover, NH03755.

Graphic Abstract:

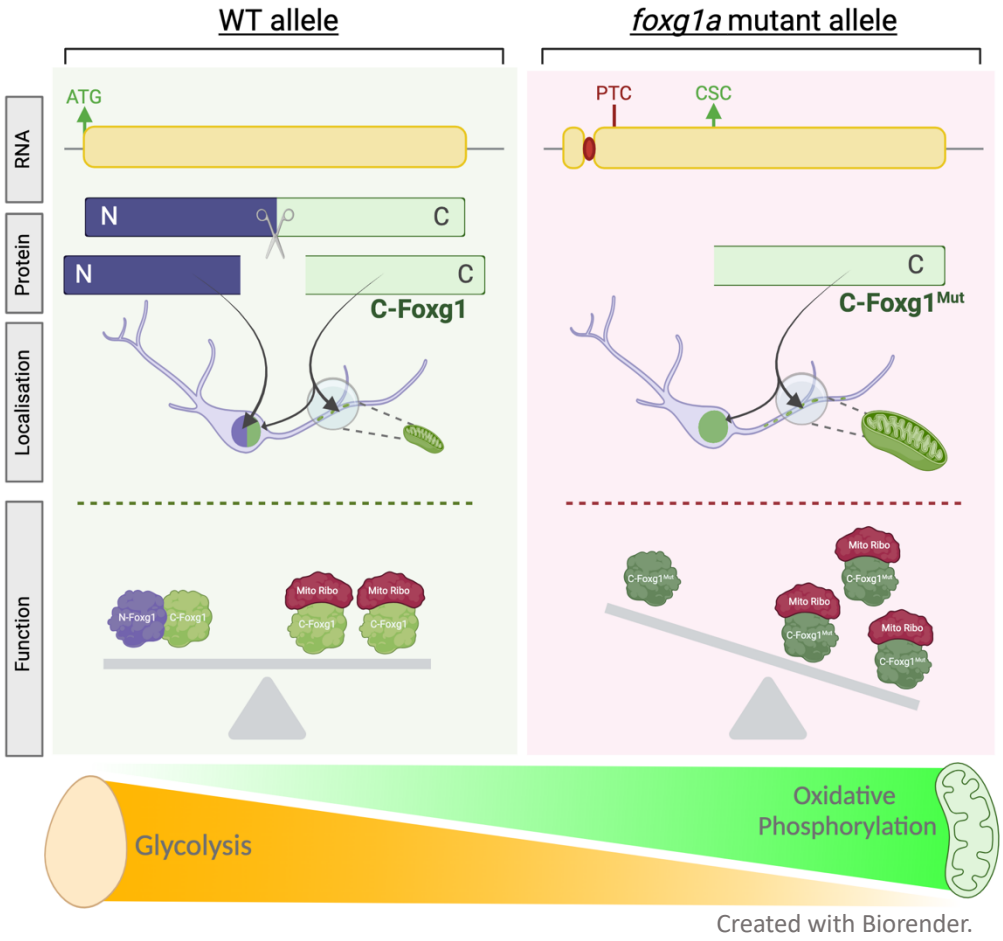

Abbreviations:

Corpus Callosum; CC, Autism Spectrum Disorder; ASD, Interneurons; IN, Excitatory/Inhibitory; E/I, Premature Termination Codon; PTC, Cryptic Start Codon; CSC, Anterior Commissure; AC, Neuronal Progenitor Cells; NPCs, Morpholino; MO, Electron Transport Chain; ETC.

bioRxiv preprint doi: https://doi.org/10.1101/2024.08.13.607559; this version posted August 13, 2024. The copyright holder for this preprint (which was not certified by peer review) is the author/funder, who has granted bioRxiv a license to display the preprint in perpetuity. It is made available under aCC-BY-NC-ND 4.0 International license.

Abstract

Modulation of mitochondrial function is at the core of cell fate decisions and tissue homeostasis, yet the mechanisms that govern their activity are not understood. Here, we provide evidence that mitochondrial activity is controlled in a tissue-specific manner through a non-canonical cytoplasmic function of the transcription factor FOXG1. Using zebrafish and human models of the neurodevelopmental disorder, FOXG1 Syndrome, we found that *FOXG1* mutations inducing a premature stop codon unexpectedly lead to the production of a short C-terminal peptide. The expression of this truncated protein is responsible for an excess of excitatory neurons and a structural, functional, and translational mitochondrial phenotype in mutants. We demonstrate that this activity is a gain of function, normally carried out by a cleavage product in wildtype. Both peptides promote the translation of mitochondrially-encoded transcripts, are preferentially transported to the mitochondria, and interact with mito-ribosomal proteins. These findings unveil a mechanism that integrates cell fate decisions with metabolic output. Adjusting the dosage of the mutant peptide rescues aspects of FOXG1 Syndrome, offering a new therapeutic avenue for the treatment of disorders involving mitochondrial dysfunctions.

Introduction

Mitochondria are known to be pivotal in cell fate decisions and have recently been identified as pacemakers in relation to species-specific development (*1*). In the context of the brain, several studies have demonstrated a shift in energy production as a cell differentiates, with stem cells reliant on glycolysis to produce ATP, while cells transitioning to neurons exhibit increased energy demand and rely on oxidative phosphorylation (*2*, *3*). Mitochondrial stimulation is known to accelerate neuronal differentiation, indicating that the organelle governs the pace of cell fate decisions (*1*, *4*). Yet, the mechanisms by which the level of mitochondrial activity is regulated during these shifts remains unknown.

Models of neurodevelopmental disease offer a valuable framework for the study of human brain development. FOXG1 Syndrome (*OMIM: 613454*) is one such disorder, caused by heterozygous disruptions in the Forkhead Box G1 (*FOXG1*) gene, which encodes a transcription factor essential for development of the telencephalon(*5*). It is predominantly characterised by microcephaly, corpus callosum (CC) agenesis, and seizures(*6*). FOXG1 dysregulation is also implicated in autism spectrum disorder (ASD) and schizophrenia (*7*, *8*). FOXG1 is amongst the earliest transcription factors to be induced in the prospective forebrain and is highly expressed in telencephalic progenitors. Homozygous deletion of *Foxg1* in mice(*5*), or *foxg1a* KD in zebrafish(*9*), leads to a drastic reduction in the size of the telencephalon as a result of premature neuronal differentiation, and depletion of the progenitor pool. As well as cortical hypoplasia, complete loss of Foxg1 results in a failure of specification of the ventral telencephalon and dorsalization of the tissue(*10*), resulting in a nearly complete loss of inhibitory interneurons (IN). Reduction of IN numbers is also observed in human FOXG1 Syndrome post-mortem cortical samples(*10*–*12*).

bioRxiv preprint doi: https://doi.org/10.1101/2024.08.13.607559; this version posted August 13, 2024. The copyright holder for this preprint (which was not certified by peer review) is the author/funder, who has granted bioRxiv a license to display the preprint in perpetuity. It is made available under aCC-BY-NC-ND 4.0 International license.

FOXG1's roles in proliferation and neuronal differentiation may be segregated across subcellular compartments. Progenitors display a predominantly nuclear localisation of FOXG1, suggesting that the transcription factor activity of the protein is required in this cell type. However, differentiating cells exhibit some cytoplasmic localisation(*13*). Furthermore, in *Xenopus*, post-translational modifications of FOXG1 influence the localisation of the protein, with phosphorylation of a serine residue (Ser 19) promoting nuclear import and phosphorylation of a threonine (Thr 226) in the C-terminus promoting nuclear export (*13*). In mouse neuronal culture, the protein can undergo post-translational cleavage producing a C-terminal fragment (C-FOXG1) that co-localizes with mitochondria and an N-terminal product that displays an exclusively nuclear localisation (*14*). Our study provides answers to the unsolved physiological functions of FOXG1 cytoplasmic localisation and cleavage products.

The majority of studies investigating FOXG1 Syndrome disease mechanisms have focused on *null* mutations which are not relevant to the human heterozygous condition. In recent years heterozygous murine models have been re-examined and advances in technology have allowed the identification of subtle proliferation deficits, axonal guidance impairment, and disruption of excitatory/inhibitory cell (E/I) balance(*15–17*). To understand the temporal dynamics of the disorder and design a vertebrate model amenable to drug screening, we produced a heterozygous *foxg1a* early frameshift zebrafish mutant. The line harbours a 5-basepair (bp) deletion close to the canonical start codon, leading to the induction of a premature termination codon (PTC, *foxg1a*$^{+/5bp}$). Similar mutations represent a third of all FOXG1 Syndrome patient genetic lesions, and these cause the most severe clinical presentations particularly in regard to seizure status(*6*).

We show *foxg1a*$^{+/5bp}$ mutants are able to recapitulate key aspects of the human condition and challenge the dogma that there is no protein expression in early PTC-generating mutations. Indeed, the zebrafish mutant mRNA adopts a downstream in-frame ATG as a cryptic start codon (CSC) to produce a C-terminal mutant Foxg1 peptide (C- Foxg1^{Mut}), a mechanism conserved in human cells. Gain and loss of C-Foxg1^{Mut} function in zebrafish shows that the peptide significantly contributes to the brain pathology in this model. We find that C-Foxg1^{Mut} is a gain of function of the normal cleavage product C-Foxg1. Both are located in the cytoplasm of neurons, more abundantly in excitatory cells and most often in mitochondria. *foxg1a*$^{+/5bp}$ mutants display a robust C-Foxg1^{Mut}-dependent mitochondrial phenotype, correlated with C-Foxg1^{Mut} cytoplasmic enrichment, and a spectacular increase in expression of mitochondrial ribosomal proteins. Our findings indicate a direct role for C-Foxg1 in mitochondrial translation, further supported by its co-immunoprecipitation with mito-ribosomal proteins.

Our study demonstrates a novel role for cytoplasmic Foxg1 in promoting neurogenesis via tuning of mitochondrial translation, providing the first evidence for direct tissue-specific instructive control of mitochondrial activity in this manner. We uncover a pathogenic gain of this mitochondrial function in fish and human disease models, unveiling a previously unknown therapeutic target and opening a potential therapeutic

bioRxiv preprint doi: https://doi.org/10.1101/2024.08.13.607559; this version posted August 13, 2024. The copyright holder for this preprint (which was not certified by peer review) is the author/funder, who has granted bioRxiv a license to display the preprint in perpetuity. It is made available under aCC-BY-NC-ND 4.0 International license.

avenue for the treatment of many disorders involving mitochondrial tuning dysfunctions.

Results

Cellular phenotype of the heterozygous *foxg1a* early frameshift mutant.

The mutation in our model results in a PTC which is situated in close proximity to the canonical start codon of the *foxg1a* gene (see methods) and is predicted to result in no protein translation. To determine the phenotype of the zebrafish *foxg1a*$^{+/5bp}$ early frameshift mutant, we used a transgenic line: (*Tg(eomesa:QF2)*^{c714} *;Tg(QUAS:mApple-CAAX; he1.1:mCherry)*^{c636} and *Tg(Dlx5a-6a;GFP)*), hereafter referred to as double transgenic. This line allows visualisation of excitatory neurons (Eomesa^{+}, aka Tbr2^{+}) via mCherry membrane labelling, while inhibitory interneurons (Dlx^{+}) can be identified by GFP whole cell labelling. At 28hpf and 48hpf the *foxg1a*$^{+/5bp}$ mutant exhibits a significant decrease in the number of inhibitory neurons and increase in the number of excitatory neurons, leading to a shift in cellular E/I balance toward excitation (Figure 1A). This change was not due to differences in the timing of neurogenesis and was already apparent soon after its onset, indicating a difference in the specification of progenitors. The possibility of compensation for this imbalance at the synapse level was ruled out by mosaic labelling of excitatory synapses (Sup. Figure 1A). Unlike mammals, the teleost telencephalon lacks a CC, with the anterior commissure (AC) being the prominent telencephalic commissure. At 28hpf there was no significant difference in the thickness, width, or volume of the AC in *foxg1a*$^{+/5bp}$ compared to *foxg1a*$^{+/+}$, suggesting that there is no developmental delay in axonal outgrowth. However, by 48hpf the thickness and volume of the AC was significantly decreased in heterozygous mutants ($p = 0.018$, unpaired t test; $p = 0.0078$, unpaired t test). Our findings were confirmed by acetylated tubulin antibody staining at 48hpf (Sup. Figure 1B), which showed a decreased thickness of the AC but no difference in the thickness of the posterior optic commissure (POC, located outside the limits of Foxg1 expression).

Microcephaly is observed in FOXG1 Syndrome patients, likely due to a depletion of progenitors from precocious neuronal differentiation. To characterise the progenitor/neuron balance in *foxg1a*$^{+/5bp}$ mutants we used a transgenic line, *Tg(HuC:GFP)*, that expresses GFP under control of the early neuronal marker ELAV3/HuC promoter and examined HuC^{+} versus HuC^{-} cells in the telencephalon(*18*). We found an early increase in numbers of post-mitotic neurons (HuC^{+}), and a

bioRxiv preprint doi: https://doi.org/10.1101/2024.08.13.607559; this version posted August 13, 2024. The copyright holder for this preprint (which was not certified by peer review) is the author/funder, who has granted bioRxiv a license to display the preprint in perpetuity. It is made available under aCC-BY-NC-ND 4.0 International license.

decreased number of progenitors (HuC^{-}), while at later stages both cell types were significantly decreased in *foxg1a*$^{+/5bp}$ mutants (Sup. Figure 1E).

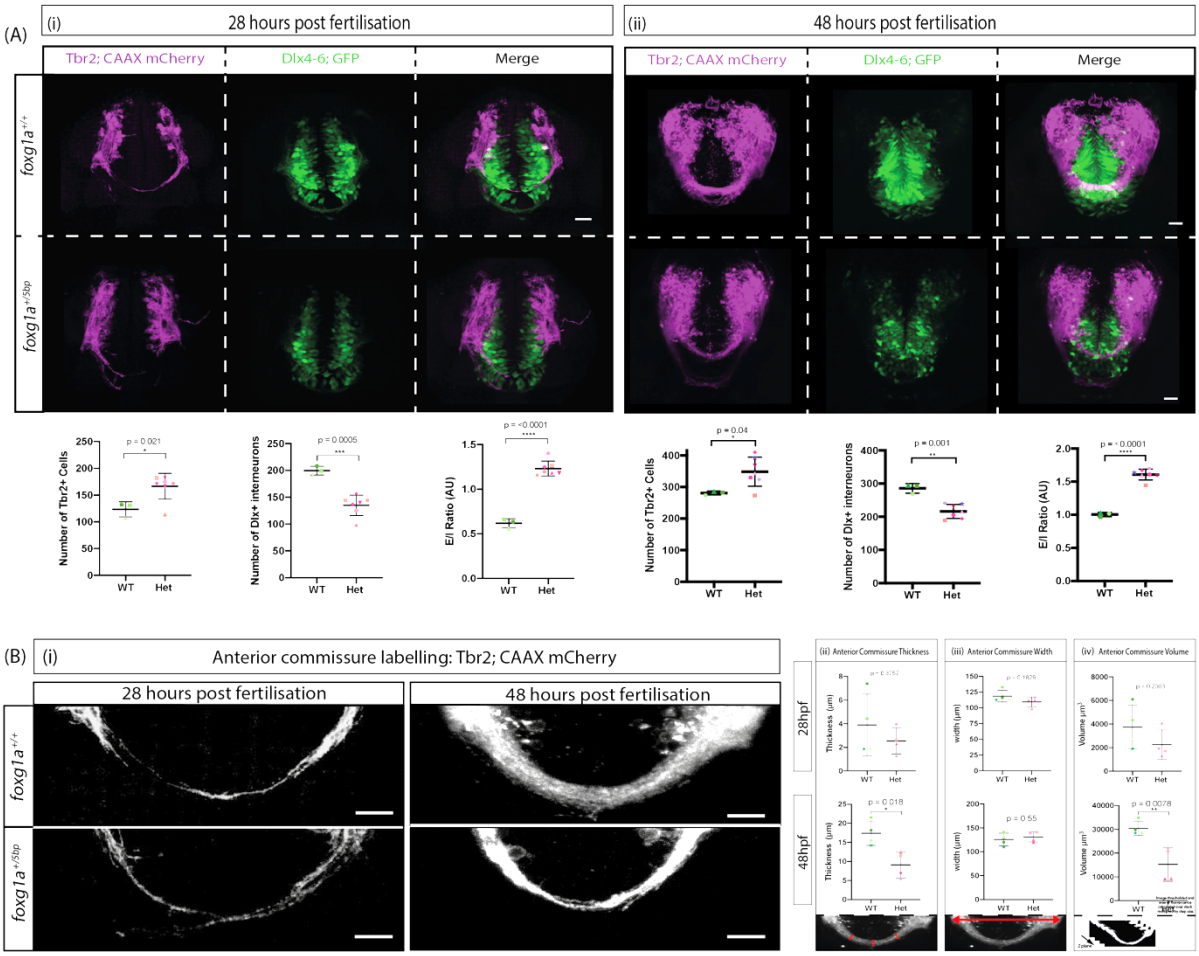

Figure 1: Phenotypic characterization of heterozygous *foxg1a*$^{+/5bp}$ mutants.

A. Representative images are projections of confocal stacks taken in a frontal view; dorsal to the top, at 28hpf (i) and 48hpf (ii) p values calculated using unpaired t test; for both stages n = 3 *foxg1a*$^{+/+}$*, 7 foxg1a*. Scale bars = 20μm; error bars indicate Standard Deviation from the Mean (SDM).

B. Representative images are projections of confocal stacks taken in a frontal view; dorsal to the top. At 28hpf and 48hpf. For both stages n = 4 *foxg1a*$^{+/+}$, 4 *foxg1a*$^{+/5bp}$, p value from unpaired t-test. Schematics under charts indicated how the measurement was performed. Scale bars = 20μm; error bars indicate SDM.

Early frameshift mutants produce a variant Foxg1 C-terminal peptide that promotes excitatory neurogenesis.

Immunostaining with a C-terminal Foxg1 antibody in the *foxg1a*$^{5bp/5bp}$ mutant unexpectedly revealed detectable protein expression in the telencephalon and nasal retina, although the signal was weaker than siblings and exhibited an altered subcellular localisation compared to *foxg1a*$^{+/+}$ (Sup. Figure 3A). Deep sequencing of

bioRxiv preprint doi: https://doi.org/10.1101/2024.08.13.607559; this version posted August 13, 2024. The copyright holder for this preprint (which was not certified by peer review) is the author/funder, who has granted bioRxiv a license to display the preprint in perpetuity. It is made available under aCC-BY-NC-ND 4.0 International license.

foxg1a$^{5bp/5bp}$ whole embryo transcriptome (Sup. Figure 2) did not support genetic compensation as an explanation for these observations. Instead, Western Blots using antibodies raised against the N or C terminus of the Foxg1 protein showed that in *foxg1a* mutants an ATG downstream of the PTC is adopted as a cryptic start codon (CSC), leading to the production of a C-terminal truncated Foxg1 (C-Foxg1^{Mut}) (Figure 2A). With the N-terminal antibody (Figure 2A ii) the *foxg1a*$^{+/+}$ and *foxg1a*$^{+/5bp}$ fish displayed bands at 50kDa (full-length Foxg1) and 30kDa (cleavage product, confirming findings in mice(*14*)), while the homozygous mutant showed no band. With the C-terminal antibody, *foxg1a*$^{+/+}$ and *foxg1a*$^{+/5bp}$ fish again displayed bands corresponding to full-length Foxg1 alongside a smaller post-translational 25kDa cleavage band. The *foxg1a*$^{+/5bp}$ and *foxg1a*$^{5bp/5bp}$ lysates additionally produced a C-terminal fragment at ~35kDa, consistent with re-initiation of translation from the first ATG downstream of the PTC (herein termed ATG4&5). Antibody staining of homozygous embryos of a CRISPR-induced line carrying a C-terminal deletion (*foxg1a*$^{\Delta C\text{-}term/\Delta C\text{-}term}$, Methods) produced no immunoreactivity, validating the band as a product of translation from CSC (Sup. Figure 4A).

Nonsense and early frameshift mutations in the N-terminus of the *FOXG1* gene are responsible for a third of all FOXG1 Syndrome mutations, giving our findings a strong translational relevance. To ask whether patient-derived telencephalic cells also produce a C-FOXG1^{Mut} peptide, we first obtained iPSCs from a patient harbouring a duplication of cysteine at position 256 (*FOXG1*$^{256DupC+/-}$), causing a frameshift and induction of a PTC (Sup. Figure 3B). However, to account for differences in genetic background, we also produced isogenic lines carrying the same mutation in a well-characterised and previously established control iPSC line (036S_CTM). We performed a dual SMAD inhibition protocol for neuronal patterning(*19*) and repeated N & C terminal antibody Western Blots on day *in vitro* 20 (DIV 20) human neuronal progenitor cells (NPCs). Control and mutant NPCs displayed bands corresponding to full-length FOXG1 (~55kDa) in both Western conditions, but mutant NPCs also produced a smaller peptide, again corresponding to re-initiation of translation from the first downstream CSC.

Given the conservation in cryptic ATG usage, we next assessed whether expression of C-Foxg1^{Mut} has functional consequences. We performed a gain of function (GOF) experiment, injecting varying doses of the mutant *foxg1a* mRNA into *foxg1a*$^{+/+}$ double transgenics (excitatory and inhibitory cell labelling) and quantified numbers of neurons at 28hpf and 56hpf. We observed a robust dose-response increase in the number of Tbr2^{+} excitatory neurons (Figure 2C) and no difference in the number of Dlx^{+} inhibitory cells, indicating that the peptide is preferentially active and/or translated in the pallium. This effect was maintained at later developmental stages (Sup. Figure 3C).

We then assessed whether repressing translation of C-Foxg1^{Mut} may improve the mutant phenotype by injection of an antisense morpholino (MO) targeting ATG4&5. Antibody staining of homozygous *foxg1a*$^{5bp/5bp}$ mutants at 24hpf confirmed that levels of protein were substantially decreased upon MO treatment (Sup. Figure 3E). When CSC function was inhibited in *foxg1a*$^{+/5bp}$ mutants at 28hpf (Sup. Figure 3D) and 56hpf (Figure 2D), Tbr2^{+} cells were significantly decreased in numbers compared to *foxg1a*$^{+/5bp}$ fish injected with a control MO ($p = 0.0003$, Two-way ANOVA). No effect

bioRxiv preprint doi: https://doi.org/10.1101/2024.08.13.607559; this version posted August 13, 2024. The copyright holder for this preprint (which was not certified by peer review) is the author/funder, who has granted bioRxiv a license to display the preprint in perpetuity. It is made available under aCC-BY-NC-ND 4.0 International license.

was observed on *Dlx+* inhibitory neurons. The decrease in excitatory cell numbers significantly improved the neuronal E/I ratio in *foxg1a*$^{+/5bp}$ embryos. We assessed the impact of the inhibition of C-Foxg1^{Mut} on the commissural phenotype at 56hpf and did not find any improvement. MO treatment had no effect on any measurement in wildtype siblings, indicating there was no effect on translation from the wildtype allele. All together, these experiments show that in the early frameshift heterozygotes, the reduction of inhibitory neurons is due to loss of full-length protein function, while the excess of excitatory neurons is a consequence of gain of function of C-Foxg1^{Mut} expression.

bioRxiv preprint doi: https://doi.org/10.1101/2024.08.13.607559; this version posted August 13, 2024. The copyright holder for this preprint (which was not certified by peer review) is the author/funder, who has granted bioRxiv a license to display the preprint in perpetuity. It is made available under aCC-BY-NC-ND 4.0 International license.

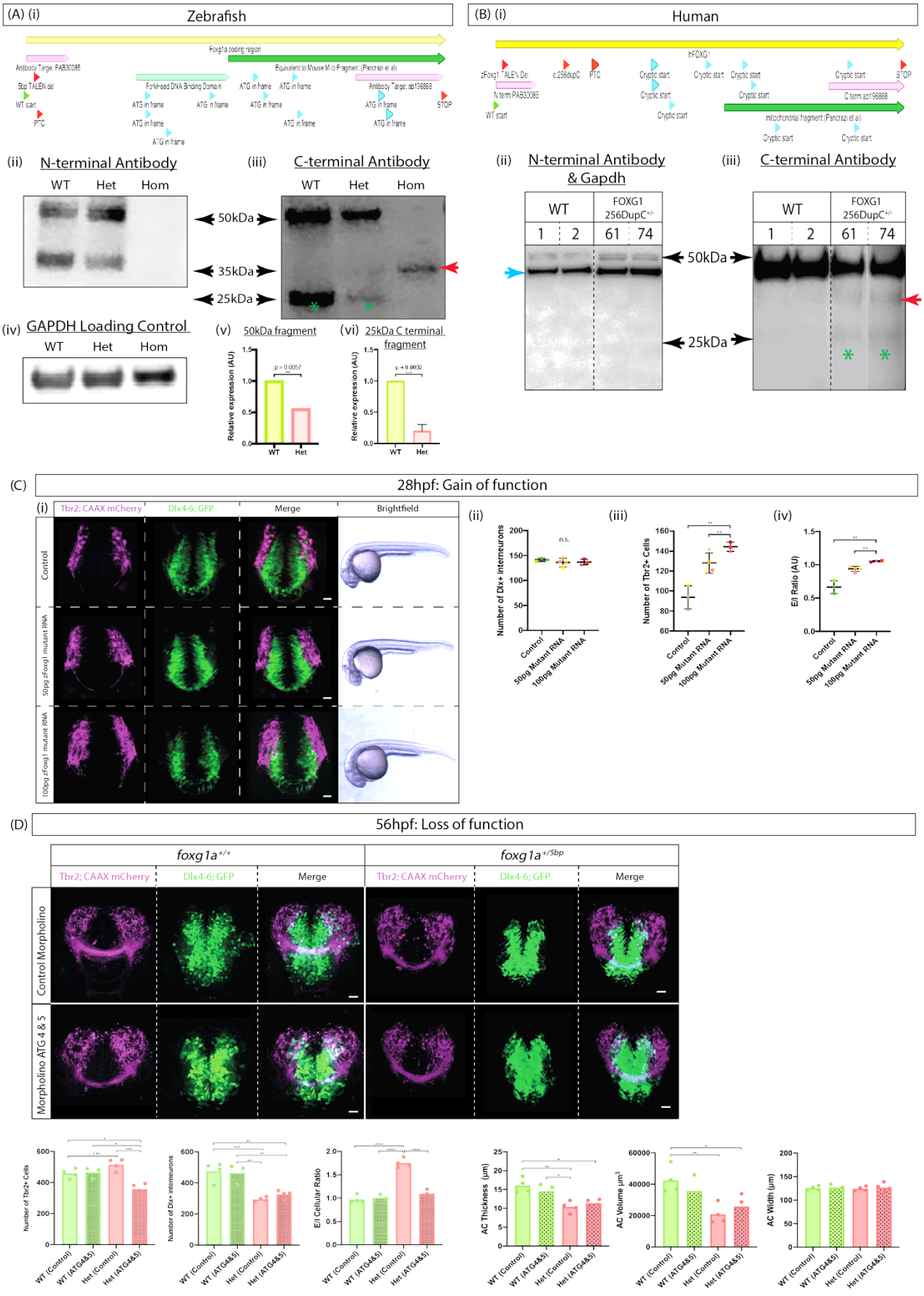

Figure 2: Re-initiation of translation from a cryptic start codon produces a variant C-terminal Foxg1.

bioRxiv preprint doi: https://doi.org/10.1101/2024.08.13.607559; this version posted August 13, 2024. The copyright holder for this preprint (which was not certified by peer review) is the author/funder, who has granted bioRxiv a license to display the preprint in perpetuity. It is made available under aCC-BY-NC-ND 4.0 International license.

(A) Zebrafish mutation and protein expression.

(i) Schematic of the zebrafish *foxg1a* gene showing 5bp TALEN deletion which causes a frameshift and the induction of a premature termination codon (PTC); further downstream are 10 ATGs in-frame with the canonical stop codon.
(ii) Western Blot on 24hpf total lysate with antibody raised against the N-terminal of Foxg1. *foxg1a*$^{+/+}$ and *foxg1a*$^{+/5bp}$ show a full-length band of ~50kDa and a smaller ~30kDa; the *foxg1a*$^{5bp/5bp}$ mutant lacks all bands.
(iii) Western Blot on 24hpf total lysate with antibody raised against the C-terminal of Foxg1. *foxg1a*$^{+/+}$ and *foxg1a*$^{+/5bp}$ show a full-length band of ~55kDa and a smaller ~25kDa; the *foxg1a*$^{+/5bp}$ and *foxg1a*$^{5bp/5bp}$ lysate has an additional band at ~35kDa.
(iv) Western Blot on 24hpf total lysate with antibody raised against Gapdh as a loading control; 50ug protein loaded per well.
(v) Quantification of the relative expression of full-length (~50kDa) Foxg1, normalized to Gapdh expression, error bars indicate SDM (n =3).
(vi) Quantification of the relative expression of wildtype cleaved C-Foxg1, normalized to Gapdh expression, error bars indicate SDM (n =3).

(B) Human mutation and protein expression.

(i) Schematic of the human *FOXG1* gene showing the patient frameshift mutation *256 duplication C*, predict to lead to PTC; further downstream are 9 ATGs in-frame with the canonical stop codon.
(ii) Western Blot on DIV 20 neuronal progenitor cells derived from two isogenic iPSC line clones (controls and *FOXG1*$^{256DupC+/-}$ mutants) with N-terminal FOXG1 antibody and GAPDH (blue arrow) as a loading control. Both control and *FOXG1* $^{+/256DupC}$ exhibit a full-length FOXG1 band at ~55kDa and GAPDH at ~37kDa. Please note an irrelevant lane was removed from between *FOXG1* $^{+/256DupC}$ Clones 61 & 74.
(iii) Western Blot on DIV 20 neuronal progenitor cells derived from iPSCs, with the C-terminal antibody. WT and *FOXG1*$^{+/256DupC}$ exhibit a full-length FOXG1 band at ~55kDa and a faint smaller band at ~25kDa. *FOXG1*$^{+/256DupC}$ and a band at ~35kDa; 50ug of protein per well. Please note an irrelevant lane was removed from between *FOXG1* $^{+/256DupC}$ Clones 61 & 74.

(C) Gain of function - Overexpression of mutant mRNA transcript in WT fish.
(i) Representative images of 28hpf controls, 50pg mutant mRNA, and 100pg mutant mRNA shown in a frontal view; scale bars= 20μm. n = 3; uninjected, 4; 50pg, 3; 100pg.
(ii) Number of Dlx^{+} interneurons; no significant difference (One-way ANOVA).
(iii) Number of Tbr2^{+} excitatory neurons; significantly increased in injected embryos *p = 0.0049* (50pg) and *p = 0.0008* (100pg), One-way ANOVA.
(iv) Excitatory/inhibitory (E/I) cellular ratio; *p= 0.001* (50pg) and *p = 0.0002* (100pg) One-way ANOVA.

(D) Loss of function - Inhibition of cryptic start codon by MO injection.
(i) Representative images of *foxg1a*$^{+/+}$ and *foxg1a*$^{+/5bp}$ 56hpf embryos injected with either a control MO or a MO against ATG4&5 (CSCs). Images are shown in a frontal view, scale bars= 20μm.
(ii) Quantification of number of Tbr2^{+} cells; Two-way ANOVA.
(iii) Quantification of number of Dlx^{+} cells; Two-way ANOVA.
(iv) Quantification of E/I cellular ratio; Two-way ANOVA.
(v) Quantification of anterior commissure (AC) thickness; Two-way ANOVA.
(vi) Quantification of AC volume; Two-way ANOVA.
(vii) Quantification of AC width; Two-way ANOVA.

bioRxiv preprint doi: https://doi.org/10.1101/2024.08.13.607559; this version posted August 13, 2024. The copyright holder for this preprint (which was not certified by peer review) is the author/funder, who has granted bioRxiv a license to display the preprint in perpetuity. It is made available under aCC-BY-NC-ND 4.0 International license.

C-Foxg1^{Mut} localises to the mitochondria and causes a bioenergetic phenotype.

Wildtype Foxg1 undergoes post-translational cleavage, with the resulting C-terminal protein (C-Foxg1) able to localise to mitochondria (*14*). We postulated that the amount of Foxg1 localising to the mitochondria may be altered in the early frameshift mutant. Using double staining with a mitochondrial marker (COX-IV), we quantified the subcellular localisation of Foxg1 and found that mutant fish exhibited an increase in the percentage of non-nuclear Foxg1, with the ATG4&5 MO injection restoring levels back to WT (Figure 3A i). To examine how much Foxg1 was localised to the mitochondria, we calculated the percentage of total Foxg1 protein and non-nuclear Foxg1 protein which localised with COX-IV. In both cases we found that *foxg1a*$^{+/5bp}$ and *foxg1a*$^{5bp/5bp}$ mutants had an increase in the percentage of Foxg1 overlapping with COX-IV and that inhibition of CSC function rescued this increase.

We also found that *foxg1a*$^{+/5bp}$ and *foxg1*$^{5bp/5bp}$ exhibit an increased mitochondrial footprint (number of mitochondria in field of view), and their mitochondria had a significantly increased mean branch length (proxy for mitochondria size, Figure 3A i). Of note, the difference between wildtype and heterozygous siblings is more pronounced in the pallium, where excitatory neurons are generated. When heterozygous mutants were treated with the MO targeting ATG4&5, the mitochondrial phenotypes were rescued, with no difference in the mitochondrial footprint or mean branch length observed between wildtype siblings and heterozygous (Figure 3A ii).
The 24hpf RNA-seq datasets (Sup. Fig.2) revealed that mitochondrially annotated differentially expressed genes (DEGs) were predominantly upregulated in mutants, with many of these including members of the electron transport chain (ETC) e.g. *ndufa6* and *cox10*. This observation suggested a functional difference in mitochondrial output, which we then examined by performing a mitochondrial stress test on 48hpf embryos. At baseline, both *foxg1a*$^{+/5bp}$ and *foxg1a*$^{5bp/5bp}$ exhibited an increase in oxygen consumption rate (OCR), compared to *foxg1a*$^{+/+}$. Similarly, when examining ATP-coupled respiration and oxidative phosphorylation, a significant increase in OCR and ATP production rate were measured in mutants. These differences were no longer apparent in populations injected with ATG4+5 MO, demonstrating that the C-Foxg1^{Mut} directly or indirectly affects mitochondrial energy production.

bioRxiv preprint doi: https://doi.org/10.1101/2024.08.13.607559; this version posted August 13, 2024. The copyright holder for this preprint (which was not certified by peer review) is the author/funder, who has granted bioRxiv a license to display the preprint in perpetuity. It is made available under aCC-BY-NC-ND 4.0 International license.

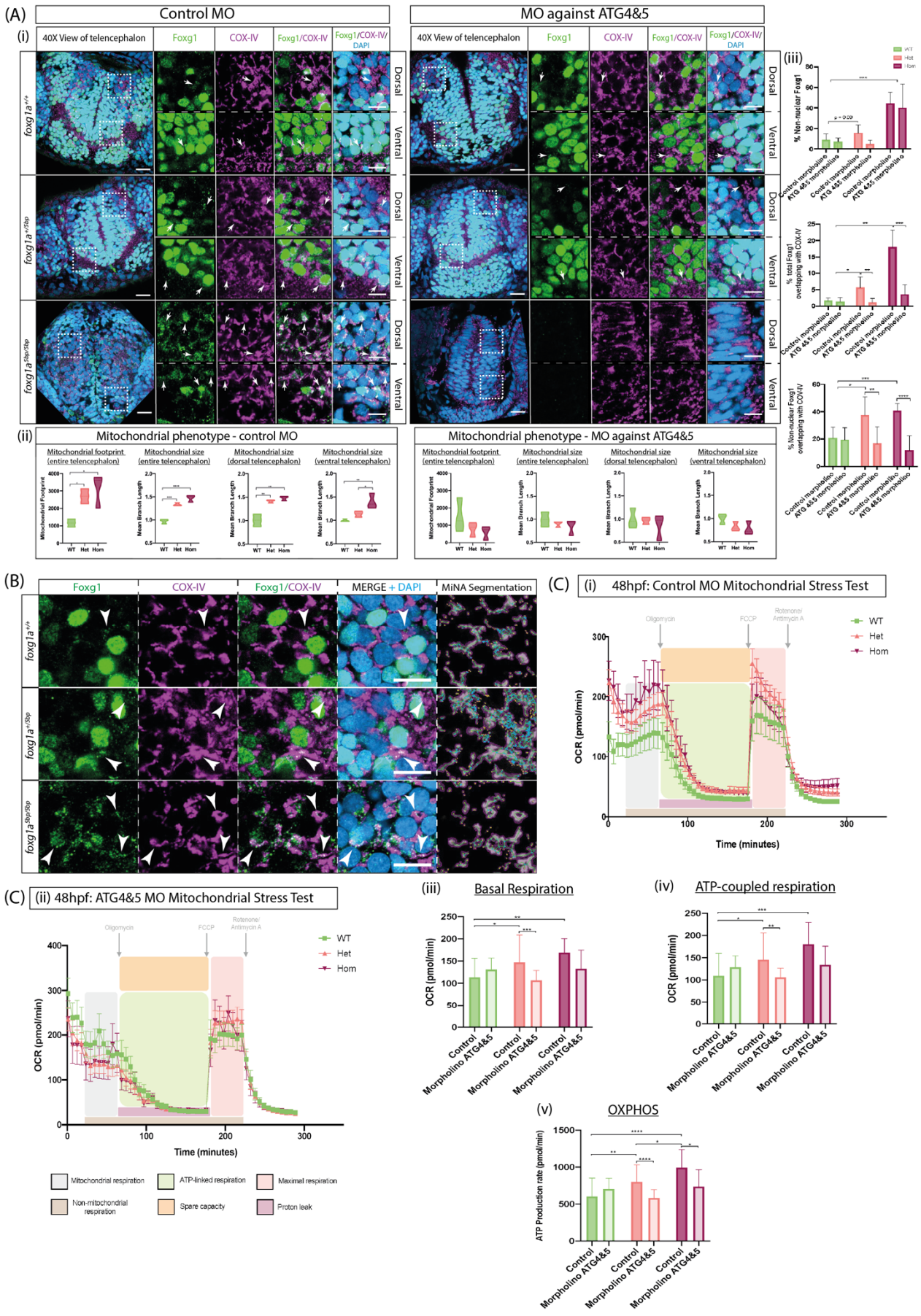

Figure 3: C-Foxg1^{Mut} modifies mitochondrial activity.

bioRxiv preprint doi: https://doi.org/10.1101/2024.08.13.607559; this version posted August 13, 2024. The copyright holder for this preprint (which was not certified by peer review) is the author/funder, who has granted bioRxiv a license to display the preprint in perpetuity. It is made available under aCC-BY-NC-ND 4.0 International license.

(A)

(i) Foxg1 and COX-IV antibody staining of 48hpf telencephalon in *foxg1a*$^{+/+}$, *foxg1a*$^{+/5bp}$ and *foxg1a*$^{5bp/5bp}$ embryos injected with a control MO or ATG4&5 MO. Representative images are single slices from a confocal stack taken in a frontal view (insets from the dorsal and ventral telencephalon). Scale bars = 20μm

(ii) Mitochondrial footprint and branch length of *foxg1a*$^{+/5bp}$ and *foxg1a*$^{5bp/5bp}$ mutants injected with control or ATG4&5 MO. Mitochondrial footprint (number of mitochondria) was increased in control morpholino treated mutants ($p = 0.005$ for *foxg1a*$^{+/5bp}$ and $p = 0.026$ for *foxg1a*$^{5bp/5bp}$, One way ANOVA). Branch length (mitochondrial size) was also significantly increased across the entire telencephalon in both mutants ($p = 0.0005$ for *foxg1a*$^{+/5bp}$ and $p = <0.0001$ for *foxg1a*$^{5bp/5bp}$, One way ANOVA). MO ATG4&5 rescued mitochondrial phenotypes in mutants. Control MO n = 3 *foxg1a*$^{+/+}$, 3 *foxg1a*$^{+/5bp}$, 3 *foxg1a*$^{5bp/5bp}$; ATG4&5 MO n = 3 *foxg1a*$^{+/+}$, 3 *foxg1a*$^{+/5bp}$, 3 *foxg1a*$^{5bp/5bp}$.

(iii) Mutant zebrafish exhibit an increase in the non-nuclear percentage of Foxg1 and an increase in the percentage of Foxg1 overlapping with the mitochondria (COX-IV). MO treatment had no effect on any measurement in WT fish but rescued the increased percentage of Foxg1 overlapping with the mitochondria in mutants. Statistics calculated with Two-way ANOVAs.

(B) High magnification view of 48hpf dorsal telencephalon mitochondria, arrows indicate areas of Foxg1 and COX-IV colocalisation. Segmentation of mitochondria by the mitochondrial network analysis tool (MiNA) is also shown. Scale bar = 10μM.

(C)

(i) Mitochondrial stress test traces for 48hpf *foxg1a*$^{+/+}$, *foxg1a*$^{+/5bp}$ and *foxg1a*$^{5bp/5bp}$ zebrafish larvae. The x axis indicates time, and the y axis indicates oxygen consumption rate (OCR) measured in pmol/min. n = 15 *foxg1a*$^{+/+}$, 34 *foxg1a*$^{+/5bp}$, and 10 *foxg1a*$^{5bp/5bp}$.

(ii) Mitochondrial stress test traces for *foxg1a*$^{+/+}$(n = 19), *foxg1a*$^{+/5bp}$ (n=31) and *foxg1a*$^{5bp\ /5bp}$ (n=10) zebrafish 48hpf larvae treated with a morpholino against ATG 4&5. .

(iii) Basal respiration measurements for control and MO treated larvae: *foxg1a*$^{+/5bp}$ and *foxg1a*$^{5bp\ /5bp}$ ($p = 0.034$ for *foxg1a*$^{+/5bp}$; $p = 0.0047$ for *foxg1a*$^{5bp/5bp}$; two-way ANOVA). ATG4/5 MO injection rescues increased respiration.

(iv) ATP-coupled respiration of *foxg1a*$^{+/5bp}$ and *foxg1a*$^{5bp\ /5bp}$ embryos injected with control or ATG4/5 MOs; $p = 0.0238$ for *foxg1a*$^{+/5bp}$; $p = 0.0004$ for *foxg1a*$^{5bp/5bp}$; two-way ANOVA).

(v) Oxidative phosphorylation (OXPHOS) of *foxg1a*$^{+/5bp}$ and *foxg1a*$^{5bp\ /5bp}$ embryos injected with control or ATG4/5; $p = 0.0043$ for *foxg1a*$^{+/5bp}$; $p = <0.0001$ for *foxg1a*$^{5bp/5bp}$; two-way ANOVA).

C-Foxg1^{Mut} interacts with ribosomal proteins and affects mitochondrial translation.

Given that the translation of transcripts encoded by the mitochondrial genome (mt-DNA) is the rate limiting step in the ETC, and that a proportion of Foxg1 is localised to the mitochondria, we postulated that C-Foxg1 may modulate translation within this organelle. The mt-DNA contains 13 protein coding genes, all of which are members of the ETC, and must be translated by a dedicated machinery that is distinct from the

bioRxiv preprint doi: https://doi.org/10.1101/2024.08.13.607559; this version posted August 13, 2024. The copyright holder for this preprint (which was not certified by peer review) is the author/funder, who has granted bioRxiv a license to display the preprint in perpetuity. It is made available under aCC-BY-NC-ND 4.0 International license.

cytosolic counterpart. A mass spectrometry study in mouse neuronal cells identified ribosomal proteins, including mitochondrial ribosomal proteins (Mrp), as potential Foxg1 interaction partners(*20*). We selected Mrps34 (Mitochondrial ribosomal protein small subunit 34) as a candidate for further exploration as this protein is central to translation activation in the mitochondria (*21*) and likely interacts with Foxg1(*20*). We performed dual co-immunoprecipitation pull downs for Mrps34 and Foxg1 (Figure 4B) from protein extracts of 24hpf WT zebrafish. When probed with an antibody against Foxg1, Western Blots of the IPs showed C-Foxg1 immunoreactivity in the Mrps34 pulldown lane (Figure 4B), demonstrating that both proteins interact in WT fish.

Wholemount immunostaining of Mrps34, revealed a dramatic increase in the area and intensity of Mrps34 expression in *foxg1a*$^{+/5bp}$ and *foxg1a*$^{5bp/5bp}$ mutants at 24hpf (Figure 4C i). Such differences in Mrps34 expression were not observed in the *foxg1a* $^{+/\Delta C\text{-}term}$ and *foxg1a* $^{\Delta C\text{-}term/\Delta C\text{-}term}$ mutants (Sup. Figure 4A). Complementarily, when *C-Foxg1-mScarlett* RNA was mosaicly overexpressed, we observed a strong positive correlation between C-Foxg1-mScarlett and Mrps34 expression (Sup. Figure 4B). Together, these results demonstrate that Mrps34 protein accumulation is dependent on the C-terminal cleavage fragment. Furthermore, the colocalisation of Foxg1 with Mrps34 was significantly increased in *foxg1a*$^{+/5bp}$ mutants, with this increase more apparent in the dorsal telencephalon i.e. the location of Tbr2^{+} excitatory neurons, Figure 4C ii. At 48hpf, a period of high neurogenesis in the wildtype telencephalon, the expression differences in Mrps34 protein were no longer significant, with strong Mrps34 expression now detected also in the wildtype siblings. Expansion microscopy on 48hpf wildtype embryos stained for Foxg1 and Mrps34 (Figure 4C iii) shows that a majority of cytoplasmic Foxg1 is mitochondrial in the wildtype pallium (Figure 4D).

We then reasoned that if Foxg1 had a role in the translation of mt-DNA encoded transcripts there would be a difference between their mRNA and protein levels. Bulk deep sequencing data from 24hpf embryos indicated that out of the 13 protein-coding genes of the mitochondrial genome, mt-Co1 and mt-Co2 transcripts were downregulated in *foxg1a* mutants. To determine if their mitochondrial translation is affected in *foxg1a*$^{+/5bp}$ mutants, we performed RNA fluorescent *in situ* hybridisation chain reaction (HCR) followed by immunostaining for mt-Co1 and Foxg1. Mutant telencephalons exhibited a decrease in the expression of mt-Co1 RNA, however, there was no significant difference in protein levels compared to WT (Figure 5E), indicating that translation of mt-Co1 is significantly increased in mutants.

bioRxiv preprint doi: https://doi.org/10.1101/2024.08.13.607559; this version posted August 13, 2024. The copyright holder for this preprint (which was not certified by peer review) is the author/funder, who has granted bioRxiv a license to display the preprint in perpetuity. It is made available under aCC-BY-NC-ND 4.0 International license.

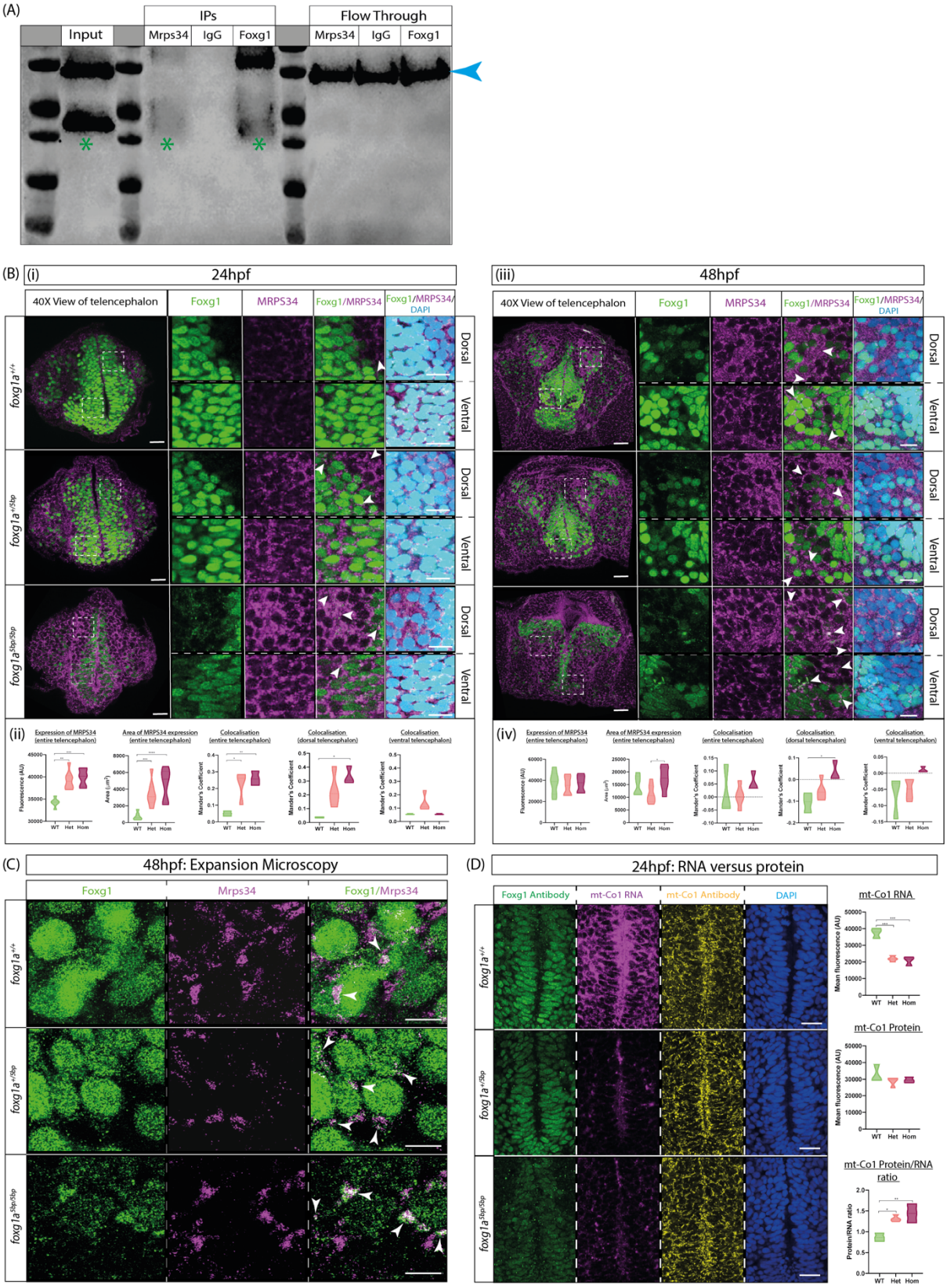

Figure 4: C-Foxg1 and C-Foxg1^{Mut} interact with mitochondrial translation machinery.

(A) Co-immunoprecipitation in *foxg1a*$^{+/+}$ fish showing that the cleaved C-Foxg1 (green asterisk) interacts with mitochondrial ribosomal protein small subunit 34 (Mrps34). Gapdh (37kDa, blue arrow) shown as a loading control. Full-length Foxg1 (50kDa) is also visible in Mrps34 IP

bioRxiv preprint doi: https://doi.org/10.1101/2024.08.13.607559; this version posted August 13, 2024. The copyright holder for this preprint (which was not certified by peer review) is the author/funder, who has granted bioRxiv a license to display the preprint in perpetuity. It is made available under aCC-BY-NC-ND 4.0 International license.

since it encompasses the C-terminal cleavage product and the IP was performed with total lysate.

(B) Wholemount immunostaining for Foxg1 and Mrps34 in 24hpf (i) and 48hpf (iii) zebrafish telencephalon; images show a frontal view with dorsal to the top, scale bars = 20μm (whole brain), 10μm (inset).
(ii) Quantification of 24hpf Mrps34 expression and colocalisation with Foxg1; *foxg1a*$^{+/+}$(n = 3), *foxg1a*$^{+/5bp}$ (n=4) and *foxg1a*$^{5bp/5bp}$ (n=3); statistics from One-way ANOVAs.
(iv)Quantification of 48hpf Mrps34 expression and colocalisation with Foxg1; *foxg1a*$^{+/+}$(n = 3), *foxg1a*$^{+/5bp}$ (n=4) and *foxg1a*$^{5bp/5bp}$ (n=3); statistics from One-way ANOVAs.

(C) Expansion microscopy of 48hpf zebrafish larvae stained for Mrps34 and Foxg1 showing colocalisation of the two, scale bars = 5μm

(D) Representative images of 24hpf *foxg1a*$^{+/+}$, *foxg1a*$^{+/5bp}$ and *foxg1a*$^{5bp/5bp}$ with mt-Col RNA (magenta), Mt-Col protein (yellow), Foxg1 protein (green), and DAPI (blue). Plots on the right are quantification of mt-Col RNA expression (top), protein expression (middle) and the ratio of protein/RNA (bottom). Statistics from One-way ANOVAs.

Mitochondrial function of C-FOXG1 is conserved from fish to human.

Since the pathology was more distinct in postmitotic neurons in zebrafish (Sup. Figure 4D) we first performed a dual SMAD inhibition protocol on *FOXG1*$^{256DupC+/-}$ and isogenic control iPSCs (036S_CTM) to produce NPCs before terminal differentiation with DAPT treatment (notch inhibition). We initially characterised the neuronal population at day 40 *in vitro* (DIV 40) and found that *FOXG1*$^{256DupC+/-}$ samples had an increase in the number of cells present in the field of view, despite an equal number of cells being seeded for terminal differentiation (Sup. Figure 5B). Immunostaining for TBR1 revealed that all neurons present in the culture were excitatory, suggesting that human C-FOXG1^{Mut} also acts to increase the number of excitatory neurons. Next, we performed immunocytochemistry for FOXG1 (C-terminal antibody) and COX-IV. Heterozygous mutant neurons exhibited an increased mitochondrial footprint compared to isogenic controls as well as an increase in mean branch length of mitochondria (Figure 5C). When examining the subcellular distribution of FOXG1, we found a trend toward increased non-nuclear localisation in *FOXG1*$^{256DupC+/-}$ neurons, and the percentage of FOXG1 protein overlapping with the mitochondria was significantly increased. An examination of expression of MRPS34 protein revealed a significant increase in *FOXG1*$^{256DupC+/-}$ neurons compared to controls (Figure 5D). Furthermore, the percentage of non-nuclear FOXG1 protein overlapping with MRPS34 was also increased in mutant neurons (Figure 5D, iii). Our findings in human neuronal cells reflect the phenotypes identified in *foxg1a* mutant zebrafish, revealing a previously unknown mitochondrial defect in FOXG1 Syndrome and the mechanism underlying these observations.

bioRxiv preprint doi: https://doi.org/10.1101/2024.08.13.607559; this version posted August 13, 2024. The copyright holder for this preprint (which was not certified by peer review) is the author/funder, who has granted bioRxiv a license to display the preprint in perpetuity. It is made available under aCC-BY-NC-ND 4.0 International license.

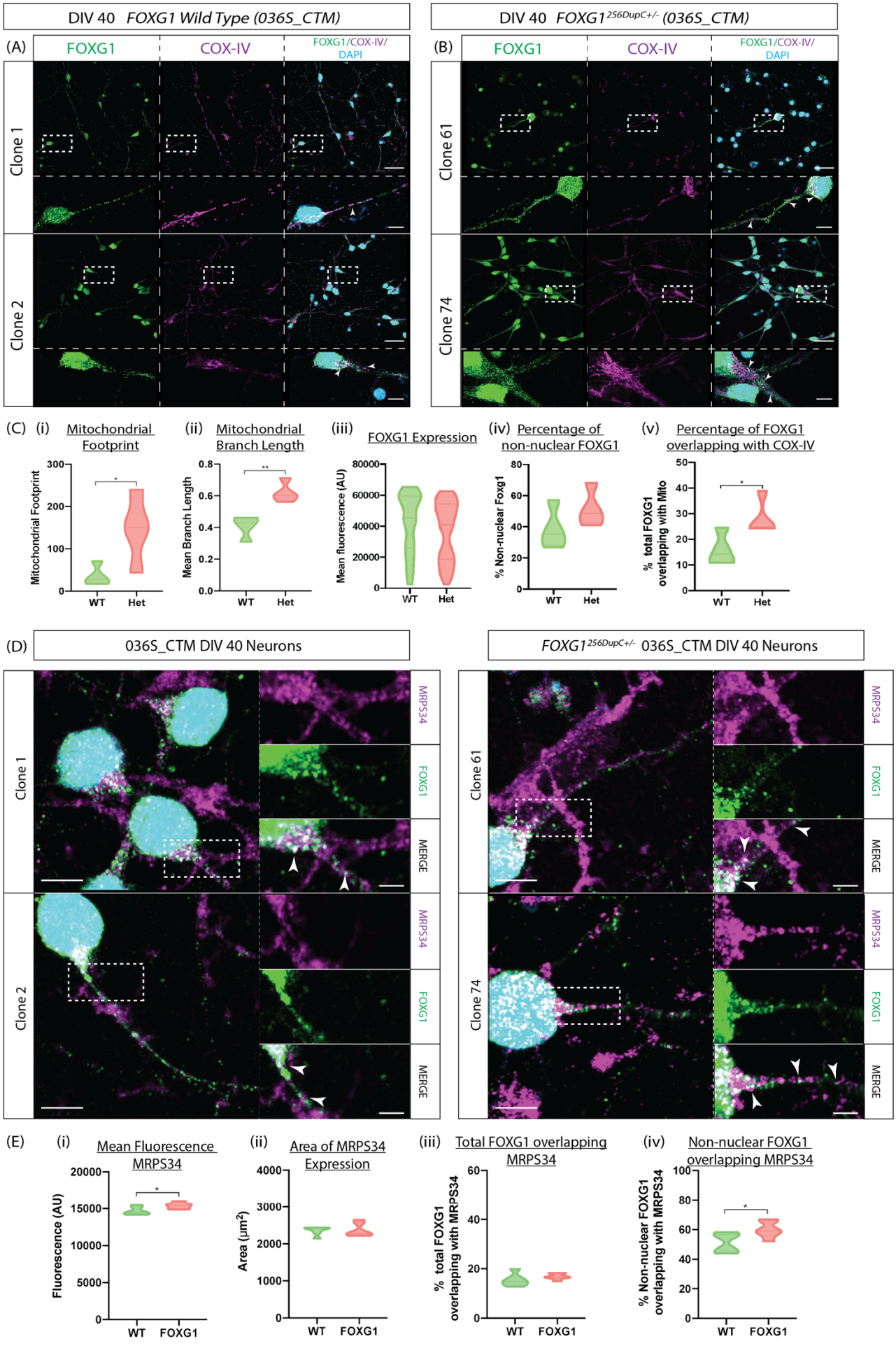

bioRxiv preprint doi: https://doi.org/10.1101/2024.08.13.607559; this version posted August 13, 2024. The copyright holder for this preprint (which was not certified by peer review) is the author/funder, who has granted bioRxiv a license to display the preprint in perpetuity. It is made available under aCC-BY-NC-ND 4.0 International license.

Figure 5: Human *FOXG1* nonsense mutant iPSC-derived neuronal cells exhibit a mitochondrial phenotype.

A & B Representative images from immunostaining for FOXG1 (green) and COX-IV (magenta) in DIV40 F*OXG1*$^{256DupC+/-}$ and isogenic control lines (036S_CTM). Dashed boxes indicate enlarged area in panel below. Scale bars = 20μm and 5μm (inset). n = 2 clones per genotype with 3 separate field of views for each clone.

C Quantification of FOXG1 and COX-IV staining all statistics from unpaired t tests.
- (i) Mitochondrial footprint measured using MiNA
- (ii) Mitochondrial branch length (mitochondria size)
- (iii) FOXG1 expression
- (iv) Percentage of non-nuclear FOXG1
- (v) Percentage of FOXG1 overlapping with COX-IV.

D Representative images from immunostaining for FOXG1 (green) and MRPS34 (magenta) in DIV40 F*OXG1*$^{256DupC+/-}$ and isogenic control lines (036S_CTM). Dashed boxes indicate enlarged area in panel to the side. Scale bars = 5μm and 2μm (inset). n = 2 clones per genotype with 3 separate field of views for each clone.

E Quantification of FOXG1 and MRPS34 staining; all statistics from unpaired t tests.
- (i) Mean fluorescence intensity of MRPS34.
- (ii) Expression area of MRPS34.
- (iii) Percentage of total FOXG1 overlapping with MRPS34
- (iv) Percentage of non-nuclear FOXG1 overlapping with MRPS34.

Discussion

This study shows that Foxg1 protein cleavage and localisation to the mitochondria is conserved from fish to humans and reveals the role of this peptide within the organelle. This function, as a regulator of mitochondrial translation, is the first of its kind to be described and provides the means to integrate decisions in specifying cell type (nuclear) with metabolic changes (mitochondrial activity).

Furthermore, our study uncovers that severe human FOXG1 syndrome mutations (frameshift and nonsense mutation early in the gene sequence) are not simply haplo-insufficient, but instead these patients suffer also from a gain of the cytoplasmic function and a loss of full-length protein activity. The gain of function is due to the adoption of a downstream CSC, leading to the translation of a truncated C-FOXG1^{Mut}, which has a pronounced impact on neurogenesis of excitatory pallial neurons. The availability of C-Foxg1^{Mut}, from early stages onwards, leads to a precocious increase in the interaction of Foxg1 with the mitochondrial translation machinery (Mrps34), resulting in a structural and functional mitochondrial phenotype. Since translation is the rate limiting step in ETC activity(*22*), we propose that the observed increase in the translation of mitochondrially encoded transcripts leads directly to the increase in oxidative phosphorylation, evidenced by our experiments.

Genotype-phenotype correlation studies have demonstrated that early nonsense or frameshift mutations in the N-terminal of FOXG1 produce the most severe phenotypes, particularly in regard to seizure status(*6*, *23*). Our results offer a molecular mechanism for this observation, since the use of CSCs is conserved from fish to human and C-Foxg1^{Mut} overexpression increases excitatory neuron numbers across

bioRxiv preprint doi: https://doi.org/10.1101/2024.08.13.607559; this version posted August 13, 2024. The copyright holder for this preprint (which was not certified by peer review) is the author/funder, who has granted bioRxiv a license to display the preprint in perpetuity. It is made available under aCC-BY-NC-ND 4.0 International license.

species. In heterozygous mutants, this excess is correlated with increased colocalisation of C-Foxg1^{Mut} with both mitochondria and Mrps34, more prominently in the dorsal telencephalon, and with a C-Foxg1^{Mut} dependent increase in mitochondrial size and activity. The dorsal abundance of cytoplasmic C-Foxg1 and C-Foxg1^{Mut}, combined with the differential impact of the latter on excitatory populations, indicate a dorsoventral regulation of protein localisation. Recent studies have indicated cell-type specific differences in the composition of the mitochondrial proteome, with excitatory and inhibitory cells exhibiting heterogenous expression of nuclear encoded mitochondrial transcripts(*24*). This work implies different cell types require a unique mitochondrial composition for their respective functions, and perhaps differentially regulated mitochondrial localisation of C-Foxg1 is in part shaping these cell type-dependent variations.

Along with changes in mitochondrial activity, neurogenesis is associated with dynamic alterations in mitochondria structure. New born neurons exhibit highly fragmented mitochondria, but maturing neurons display fused mitochondria(*4*). In the context of our results, which demonstrated an increase in the mean branch length of neuronal mitochondria, this suggests that mutant neurons are more mature in comparison to WT, supporting the observation of a premature differentiation phenotype in FOXG1 Syndrome. Furthermore, antisense inhibition of C-Foxg1^{Mut} rescued the increased mitochondrial footprint, mean branch length, and functional output of the mitochondria in mutant fish, allowing us to conclude that C-Foxg1^{Mut} is responsible for these phenotypes. The proper function of the ETC is essential for efficient ATP output via oxidative phosphorylation, requiring appropriate regulation of translation within the mitochondria. Mutations in genes encoding mitochondrial translation machinery are associated with multiple neurodevelopmental phenotypes such as intellectual disability, seizures, myelination, and abnormal volume/structure of the CC (*21*, *25*, *26*). Interestingly, mitochondrial ribosomal subunits appear to be developmentally regulated with an increased expression from birth, before a peak at ~5.5 years, which also happens to correspond to the average age of susceptibility of neurodevelopmental disorders (*27*, *28*). Yet, the mechanism regulating mitochondrial translation is not yet fully understood. The only mitochondria-specific translation activator identified to date is TACO1, promoting ribosomal translation initiation through interaction with Mrps34(*29*). C-FOXG1 is the first spatio-temporal regulator of mitochondrial translation identified, providing the means to start dissecting the telencephalic mechanism of mitochondrial translation control at cell type resolution.

This work uncovers a previously unknown therapeutic target that extends beyond FOXG1 Syndrome itself, as mitochondrial C-FOXG1 is also likely to play a role in other disorders where FOXG1 is mis-regulated e.g. ASD & schizophrenia, and may become a useful therapeutic tool in conditions of mitochondrial dysfunctions. Our findings open even wider avenues for investigation as nonsense mutations account for around 11% of all disease-causing mutations in humans(*30*). Preliminary examination of related genes (*MECP2* and *CDKL5*) has highlighted multiple potential CSCs downstream from reported nonsense mutations in patients. Future work will aim to further characterise the role of C-Foxg1 and C-Foxg1^{Mut} in the regulation of mitochondrial translation in fish and humans and understand the mechanism underlying the cleavage of Foxg1 and subsequent import into the mitochondria. Ultimately, as demonstrated by

bioRxiv preprint doi: https://doi.org/10.1101/2024.08.13.607559; this version posted August 13, 2024. The copyright holder for this preprint (which was not certified by peer review) is the author/funder, who has granted bioRxiv a license to display the preprint in perpetuity. It is made available under aCC-BY-NC-ND 4.0 International license.

experiments that repress mutant phenotypes, such studies could lead to the development of new antisense therapeutics for the human disorder.

bioRxiv preprint doi: https://doi.org/10.1101/2024.08.13.607559; this version posted August 13, 2024. The copyright holder for this preprint (which was not certified by peer review) is the author/funder, who has granted bioRxiv a license to display the preprint in perpetuity. It is made available under aCC-BY-NC-ND 4.0 International license.

References:

1. R. Iwata, P. Casimir, E. Erkol, L. Boubakar, M. Planque, I. M. Gallego López, M. Ditkowska, V. Gaspariunaite, S. Beckers, D. Remans, K. Vints, A. Vandekeere, S. Poovathingal, M. Bird, I. Vlaeminck, E. Creemers, K. Wierda, N. Corthout, P. Vermeersch, S. Carpentier, K. Davie, M. Mazzone, N. V. Gounko, S. Aerts, B. Ghesquière, S. M. Fendt, P. Vanderhaeghen, Mitochondria metabolism sets the species-specific tempo of neuronal development. *Science (80-.).* **379** (2023).
2. X. Zheng, L. Boyer, M. Jin, J. Mertens, Y. Kim, L. Ma, L. Ma, M. Hamm, F. H. Gage, T. Hunter, Metabolic reprogramming during neuronal differentiation from aerobic glycolysis to neuronal oxidative phosphorylation. *Elife* **5** (2016).
3. M. Agathocleous, N. K. Love, O. Randlett, J. J. Harris, J. Liu, A. J. Murray, W. A. Harris, Metabolic differentiation in retinal cells. *Nat. Rev. Mol. Cell Biol.* **14** (2013).
4. R. Iwata, P. Casimir, P. Vanderhaeghen, Mitochondrial dynamics in postmitotic cells regulate neurogenesis. *Science (80-.).* **369** (2020).
5. S. Xuan, C. A. Baptista, G. Balas, W. Tao, V. C. Soares, E. Lai, Winged helix transcription factor BF-1 is essential for the development of the cerebral hemispheres. *Neuron* **14**, 1141–52 (1995).
6. D. Mitter, M. Pringsheim, M. Kaulisch, D. Pol, K. Sarah Plümacher, S. Schröder, R. Warthemann, R. Abou Jamra, M. Baethmann, T. Bast, H.-M. Büttel, J. S. Cohen, E. Conover, C. Courage, A. Eger, A. Fatemi, T. A. Grebe, N. S. Hauser, W. Heinritz, K. L. Helbig, M. Heruth, D. Huhle, K. Höft, S. Karch, G. Kluger, G. Christoph Korenke, J. R. Lemke, R. E. Lutz, S. Patzer, I. Prehl, D. Biol, K. Hoertnagel, K. Ramsey, T. Rating, A. Rieß, L. Rohena, M. Schimmel, R. Westman, F.-M. Zech, B. Zoll, D. Malzahn, B. Zirn, K. Brockmann, FOXG1 syndrome: genotype–phenotype association in 83 patients with FOXG1 variants. *Genet. Med.* **20** (2018).
7. J. Mariani, G. Coppola, P. Zhang, A. Abyzov, L. Provini, L. Tomasini, M. Amenduni, A. Szekely, D. Palejev, M. Wilson, M. Gerstein, E. L. Grigorenko, K. Chawarska, K. A. Pelphrey, J. R. Howe, F. M. Vaccarino, FOXG1-Dependent Dysregulation of GABA/Glutamate Neuron Differentiation in Autism Spectrum Disorders. *Cell* **162**, 375–390 (2015).
8. H. Won, L. de la Torre-Ubieta, J. L. Stein, N. N. Parikshak, J. Huang, C. K. Opland, M. J. Gandal, G. J. Sutton, F. Hormozdiari, D. Lu, C. Lee, E. Eskin, I. Voineagu, J. Ernst, D. H. Geschwind, Chromosome conformation elucidates regulatory relationships in developing human brain. *Nature* **538**, 523–527 (2016).
9. C. Danesin, J. N. Peres, M. Johansson, V. Snowden, A. Cording, N. Papalopulu, C. Houart, Integration of Telencephalic Wnt and Hedgehog Signaling Center Activities by Foxg1. *Dev. Cell* **16**, 576–587 (2009).
10. B. Martynoga, H. Morrison, D. J. Price, J. O. Mason, Foxg1 is required for specification of ventral telencephalon and region-specific regulation of dorsal telencephalic precursor proliferation and apoptosis. *Dev. Biol.* **283**, 113–127 (2005).
11. S. Huh, V. Hatini, R. C. Marcus, S. C. Li, E. Lai, Dorsal–Ventral Patterning Defects in the Eye of BF-1-Deficient Mice Associated with a Restricted Loss of shh Expression. *Dev. Biol.* **211**, 53–63 (1999).

bioRxiv preprint doi: https://doi.org/10.1101/2024.08.13.607559; this version posted August 13, 2024. The copyright holder for this preprint (which was not certified by peer review) is the author/funder, who has granted bioRxiv a license to display the preprint in perpetuity. It is made available under aCC-BY-NC-ND 4.0 International license.

12. N. M. Wilpert, F. Marguet, C. Maillard, F. Guimiot, J. Martinovic, S. Drunat, T. Attié-Bitach, F. Razavi, A. Tessier, Y. Capri, A. Laquerrière, N. Bahi-Buisson, Human neuropathology confirms projection neuron and interneuron defects and delayed oligodendrocyte production and maturation in FOXG1 syndrome. *Eur. J. Med. Genet.* **64** (2021).
13. T. Regad, M. Roth, N. Bredenkamp, N. Illing, N. Papalopulu, The neural progenitor-specifying activity of FoxG1 is antagonistically regulated by CKI and FGF. *Nat. Cell Biol.* **9**, 531–540 (2007).
14. L. Pancrazi, G. Di Benedetto, L. Colombaioni, G. Della Sala, G. Testa, F. Olimpico, A. Reyes, M. Zeviani, T. Pozzan, M. Costa, Foxg1 localizes to mitochondria and coordinates cell differentiation and bioenergetics. *Proc. Natl. Acad. Sci. U. S. A.* **112**, 13910–5 (2015).
15. K. L. Eagleson, L. J. Schlueter McFadyen-Ketchum, E. T. Ahrens, P. H. Mills, M. D. Does, J. Nickols, P. Levitt, Disruption of Foxg1 expression by knock-in of Cre recombinase: Effects on the development of the mouse telencephalon. *Neuroscience* **148**, 385–399 (2007).
16. M. Pringsheim, D. Mitter, S. Schröder, R. Warthemann, K. Plümacher, G. Kluger, M. Baethmann, T. Bast, S. Braun, H. M. Büttel, E. Conover, C. Courage, A. N. Datta, A. Eger, T. A. Grebe, A. Hasse-Wittmer, M. Heruth, K. Höft, A. M. Kaindl, S. Karch, T. Kautzky, G. C. Korenke, B. Kruse, R. E. Lutz, H. Omran, S. Patzer, H. Philippi, K. Ramsey, T. Rating, A. Rieß, M. Schimmel, R. Westman, F. M. Zech, B. Zirn, P. A. Ulmke, G. Sokpor, T. Tuoc, A. Leha, M. Staudt, K. Brockmann, Structural brain anomalies in patients with FOXG1 syndrome and in Foxg1+/– mice. *Ann. Clin. Transl. Neurol.* **6** (2019).
17. F. Cargnin, J.-S. Kwon, S. Katzman, B. Chen, J. W. Lee, S.-K. Lee, FOXG1 Orchestrates Neocortical Organization and Cortico-Cortical Connections. *Neuron* **100**, 1083-1096.e5 (2018).
18. C. H. Kim, E. Ueshima, O. Muraoka, H. Tanaka, S. Y. Yeo, T. L. Huh, N. Miki, Zebrafish elav/HuC homologue as a very early neuronal marker. *Neurosci. Lett.* **216** (1996).
19. S. M. Chambers, C. A. Fasano, E. P. Papapetrou, M. Tomishima, M. Sadelain, L. Studer, Highly efficient neural conversion of human ES and iPS cells by dual inhibition of SMAD signaling. *Nat. Biotechnol.* **27**, 275–280 (2009).
20. S. C. Weise, G. Arumugam, A. Villarreal, P. Videm, S. Heidrich, N. Nebel, V. I. Dumit, F. Sananbenesi, V. Reimann, M. Craske, O. Schilling, W. R. Hess, A. Fischer, R. Backofen, T. Vogel, FOXG1 Regulates PRKAR2B Transcriptionally and Posttranscriptionally via miR200 in the Adult Hippocampus. *Mol. Neurobiol.* **56** (2019).
21. N. J. Lake, B. D. Webb, D. A. Stroud, T. R. Richman, B. Ruzzenente, A. G. Compton, H. S. Mountford, J. Pulman, C. Zangarelli, M. Rio, N. Bodaert, Z. Assouline, M. D. Sherpa, E. E. Schadt, S. M. Houten, J. Byrnes, E. M. McCormick, Z. Zolkipli-Cunningham, K. Haude, Z. Zhang, K. Retterer, R. Bai, S. E. Calvo, V. K. Mootha, J. Christodoulou, A. Rötig, A. Filipovska, I. Cristian, M. J. Falk, M. D. Metodiev, D. R. Thorburn, Biallelic Mutations in MRPS34 Lead to Instability of the Small Mitoribosomal Subunit and Leigh Syndrome. *Am. J. Hum. Genet.* **101** (2017).
22. D. F. Bogenhagen, J. D. Haley, Pulse-chase SILAC- based analyses reveal selective oversynthesis and rapid turnover of mitochondrial protein

bioRxiv preprint doi: https://doi.org/10.1101/2024.08.13.607559; this version posted August 13, 2024. The copyright holder for this preprint (which was not certified by peer review) is the author/funder, who has granted bioRxiv a license to display the preprint in perpetuity. It is made available under aCC-BY-NC-ND 4.0 International license.

components of respiratory complexes. (2020). https://doi.org/10.1074/jbc.RA119.011791.

23. L. E. Seltzer, M. Ma, S. Ahmed, M. Bertrand, W. B. Dobyns, J. Wheless, A. R. Paciorkowski, Epilepsy and outcome in FOXG1-related disorders. *Epilepsia* **55**, 1292–1300 (2014).
24. M. E. Wynne, A. R. Lane, K. S. Singleton, S. A. Zlatic, A. Gokhale, E. Werner, D. Duong, J. Q. Kwong, A. J. Crocker, V. Faundez, Heterogeneous expression of nuclear encoded mitochondrial genes distinguishes inhibitory and excitatory neurons. *eNeuro* **8** (2021).
25. C. R. Coughlin, G. H. Scharer, M. W. Friederich, H. C. Yu, E. A. Geiger, G. Creadon-Swindell, A. E. Collins, A. V. Vanlander, R. Van Coster, C. A. Powell, M. A. Swanson, M. Minczuk, J. L. K. van Hove, T. H. Shaikh, Mutations in the mitochondrial cysteinyl-tRNA synthase gene, CARS2, lead to a severe epileptic encephalopathy and complex movement disorder. *J. Med. Genet.* **52** (2015).
26. P. Devaraju, J. Yu, D. Eddins, M. M. Mellado-Lagarde, L. R. Earls, J. J. Westmoreland, G. Quarato, D. R. Green, S. S. Zakharenko, Haploinsufficiency of the 22q11.2 microdeletion gene Mrpl40 disrupts short-term synaptic plasticity and working memory through dysregulation of mitochondrial calcium. *Mol. Psychiatry* **22** (2017).
27. P. Bülow, A. Patgiri, V. Faundez, Mitochondrial protein synthesis and the bioenergetic cost of neurodevelopment. (2022). https://doi.org/10.1016/j.isci.2022.104920.
28. M. Solmi, J. Radua, M. Olivola, E. Croce, L. Soardo, G. Salazar de Pablo, J. Il Shin, J. B. Kirkbride, P. Jones, J. H. Kim, J. Y. Kim, A. F. Carvalho, M. V. Seeman, C. U. Correll, P. Fusar-Poli, Age at onset of mental disorders worldwide: large-scale meta-analysis of 192 epidemiological studies. (2022). https://doi.org/10.1038/s41380-021-01161-7.
29. T. R. Richman, H. Spahr, J. A. Ermer, S. M. K. Davies, H. M. Viola, K. A. Bates, J. Papadimitriou, L. C. Hool, J. Rodger, N. G. Larsson, O. Rackham, A. Filipovska, Loss of the RNA-binding protein TACO1 causes late-onset mitochondrial dysfunction in mice. *Nat. Commun.* **7** (2016).
30. M. Mort, D. Ivanov, D. N. Cooper, N. A. Chuzhanova, A meta-analysis of nonsense mutations causing human genetic disease. *Hum. Mutat.* **29** (2008).
31. M. Yu, Y. Xi, J. Pollack, M. Debiais-Thibaud, R. B. MacDonald, M. Ekker, Activity of dlx5a/dlx6a regulatory elements during zebrafish GABAergic neuron development. *Int. J. Dev. Neurosci.* **29** (2011).
32. S. M. Asano, R. Gao, A. T. Wassie, P. W. Tillberg, F. Chen, E. S. Boyden, Expansion Microscopy: Protocols for Imaging Proteins and RNA in Cells and Tissues. *Curr. Protoc. Cell Biol.* **80** (2018).
33. S. Bolte, F. P. Cordelières, A guided tour into subcellular colocalization analysis in light microscopy. (2006). https://doi.org/10.1111/j.1365-2818.2006.01706.x.
34. A. J. Valente, L. A. Maddalena, E. L. Robb, F. Moradi, J. A. Stuart, A simple ImageJ macro tool for analyzing mitochondrial network morphology in mammalian cell culture. *Acta Histochem.* **119** (2017).
35. R. Ibarra-García-Padilla, A. G. A. Howard, E. W. Singleton, R. A. Uribe, A protocol for whole-mount immuno-coupled hybridization chain reaction

bioRxiv preprint doi: https://doi.org/10.1101/2024.08.13.607559; this version posted August 13, 2024. The copyright holder for this preprint (which was not certified by peer review) is the author/funder, who has granted bioRxiv a license to display the preprint in perpetuity. It is made available under aCC-BY-NC-ND 4.0 International license.

(WICHCR) in zebrafish embryos and larvae. *STAR Protoc.* **2** (2021).
36. lukemiller.org» Blog Archive » Analyzing gels and western blots with ImageJ. https://lukemiller.org/index.php/2010/11/analyzing-gels-and-western-blots-with-image-j/.
37. Y. Wang, C. Wang, P. Ranefall, G. J. Broussard, Y. Wang, G. Shi, B. Lyu, C.-T. Wu, W. Yue, L. Tian, G. Yu, SynQuant: A Fiji plugin that automatically quantify synapses from multi-channel fluorescence microscopy images. *Bioinformatics* **36**, 1599–1606 (2020).
38. V. Madhu, A. S. Dighe, Q. Cui, D. N. Deal, Dual inhibition of activin/nodal/tgf- β and bmp signaling pathways by sb431542 and dorsomorphin induces neuronal differentiation of human adipose derived stem cells. *Stem Cells Int.* **2016** (2016).

Acknowledgements

We would like to thank Michelle Macurak (MEH lab), who produced the (*Tg(eomesa:QF2)*^{c714} *;Tg(QUAS:mApple-CAAX; he1.1:mCherry)*^{c636} line; Oscar Marin for his comments and feedback on the manuscript; Kathryn Adamson for her help in reviewing the paper prior to submission; and Graham Cocks for his production of the isogenic iPSC lines used in this study. We would also like to acknowledge Biorender.com, which was used to produce the graphic abstract for this work. This work is supported by funds from the Wellcome Trust (WT 220861/Z/20/Z to CH) and Medical Research Council (MR/N026063/1 to HB).

Author Contributions:

Conceptualization, HB & CH. Methodology, HB. Investigation, HB. Experimental work, HB. Image analysis, HB. RNA-sequencing data analysis, FH. Visualization, HB. Production of (*Tg(eomesa:QF2)*^{c714} *;Tg(QUAS:mApple-CAAX; he1.1:mCherry)*^{c636} line, MEH. Production of *foxg1a*$^{+/5bp}$ line, CM & OS. Production of C-terminal deletion line, HB. Writing, review and editing, HB and CH. Supervision, CH. Funding acquisition, HB and CH.

Declaration of Interests

The authors declare that they have no known competing financial interests or personal relationships that could have appeared to influence the work reported in this article.

bioRxiv preprint doi: https://doi.org/10.1101/2024.08.13.607559; this version posted August 13, 2024. The copyright holder for this preprint (which was not certified by peer review) is the author/funder, who has granted bioRxiv a license to display the preprint in perpetuity. It is made available under aCC-BY-NC-ND 4.0 International license.

Supplementary Materials

Materials and Methods

Zebrafish Husbandry

All fish used in this project were cared for and raised at the Guy's Campus Zebrafish facility,King's College London. Embryos for experimental analysis were collected from adult zebrafish pairings and incubated at 28.5^{o}C in fish system water containing 0.01% methylene blue; to minimise pigment formation 0.003% 1-phenyl-2-thiourea (PTU) was added to the fish water. The local Animal Care and Use Committee at King's College London approved all fish work in this study, which was carried out under licenses issued by the Home Office and experiments were carried out in accordance with the Animals in Scientific Procedures Act of 1986. The *foxg1a* nonsense mutation used in this study was achieved by a TALEN (transcription activator-like nucleases) deletion of 5 base pairs (bp) near the start codon of the *foxg1a* coding region; this deletion results in a frameshift and the induction of an early stop codon. TALEN technology predates the recent CRISPR-Cas9 advances in genome editing and relies on the generation of a gene-specific TAL effector DNA binding domain fused to a DNA cleavage domain to mediate double stranded DNA breaks (Nemudryi et al., 2014). As the *foxg1a* homozygous mutant fish dies 8-10 days post fertilisation (dpf), adult fish stocks were maintained as heterozygous carriers. Progeny from heterozygous incrosses were genotyped by PCR amplification and subsequent sanger sequencing, genotype was determined by the deletion of 5bp.

Adult Zebrafish

Finclips from adult fish were digested overnight at 55^{o}C in 50µl DNA extraction buffer (*100mM Tris-HCL pH8.5, 5mM EDTA pH 8.0, 200mM NaCl, 0.2% SDS*) supplemented with 100µg/ml Proteinase K. The following morning the Proteinase K was heat-inactivated at 85^{o}C for 45 minutes; DNA was diluted 1:10 in molecular grade H_20 and 1µl was used as a template in a 25µl PCR reaction (F – GAGGAGTTGCCAGAGCAAG, R – GCCGTTTTTCTTGTCGCCTT) using DreamTaq Green PCR Mastermix (*Thermofisher*, K1081).

Zebrafish Larvae

Larvae up to 6dpf were genotyped by alkaline lysis DNA extraction in 45µl of solution (*25mM NaOH, 0.2mM EDTA*), heated to 95^{o}C for one hour; 50µl of neutralisation buffer (*40mM Tris-HCL pH8.0*) was then added and 1µl was then used as DNA template in a PCR reaction.

Genotyping of Fixed Zebrafish Larvae

Following in situ hybridisation or wholemount immunostaining, fixed embryos were genotyped after imaging by DNA extraction from the tails of the embryo. Tails were digested overnight at 55oC in 30µl of Fixed Sample DNA Extraction Buffer (*50mM KCl, 10mM Tris-HCL pH8.3, 0.3% TWEEN-20, 0.3% NP40*) supplemented with

bioRxiv preprint doi: https://doi.org/10.1101/2024.08.13.607559; this version posted August 13, 2024. The copyright holder for this preprint (which was not certified by peer review) is the author/funder, who has granted bioRxiv a license to display the preprint in perpetuity. It is made available under aCC-BY-NC-ND 4.0 International license.

100µg/ml Proteinase K. The following morning the Proteinase K was heat-inactivated as before, and 2µl was used in 25µl pcr reaction. Following PCR, samples were checked on a 1% Agarose gel with ethidium bromide staining and sent for sequencing with the forward primer using Eurofins Mix2Seq Overnight Sequencing Service.

Zebrafish Lines

The transgenic lines used in this study were obtained by crossing heterozygous *foxg1a* mutants with the established transgenics; details of each transgenic line can be found in table 1.

Table 1: Details of zebrafish lines utilised in this study.

Line Na	Description	Ref (if applicable)
Foxg1 TALEN x (*Tg(eomesa:QF2)^{c714} ;Tg(QUAS:mApple-CAAX; he1.1:mCherry)^{c636} and Tg(1.1Dlxa5-6a;GFP*)	Labels the membranes of Tbr2+ excitatory cells in the pallium. Whole cell GFP labelling of Dlx+ neurons.	(*Tg(eomesa:QF2)^{c714} ;Tg(QUAS:mApple-CAAX; he1.1:mCherry)^{c636}* portion was produced by Michelle Macurak of Marnie E. Halpern's lab. *Tg(1.1Dlxa5-6a;GFP*)) was produced by Mark Ekker's group. (*31*)
Foxg1 TALEN x *Tg(HuC;GFP)*	Labelling of post mitotic neurons	NA
Foxg1 TALEN	5bp TALEN deletion causing a frameshift and PTC.	Houart Lab
Foxg1 C-terminal Deletion	CRISPR Cas9-mediated deletion of the C-terminal of *foxg1a*	Houart Lab

Generation of C-terminal deletion CRISPR Cas9 mutant

Integrated DNA technologies (IDT) online CRSIPR sgRNA analysis was used to determine the predicted efficiency of multiple guide RNAs, and two with the best scores were ordered as crRNA (sgRNA3; *ATACACTAACTAGCATCCAC* and sgRNA4; *TCACTTACAGTCTGATCCTG*). Lyophilised crRNAs and tracrRNA were reconstituted to 200μm in IDT duplex buffer. crRNAs were annealed with tracrRNA (IDT, 1072532) by combining 1μl of each sgRNA, 1μl of tracrRNA, and 0.28μl duplex buffer in a PCR tube and heating to 95^{o}C for 5 mins before cooling to RT. 1μl of the resultant sgRNA complexes (61μM) were combined with 1μl of Cas9 protein (IDT, 1081058) and heated at 37^{o}C for 5 mins to produce a ribonucleoprotein complex. Embryos at the one-cell stage were then injected with 1nl of this solution diluted 1/10 in dH_2O. Mutation frequency was checked by PCR (F; *TTTGTGGCTACCTTAGAGTCC*, R; *ATTCGGCTTGCATTGTCCGTTC*), with

bioRxiv preprint doi: https://doi.org/10.1101/2024.08.13.607559; this version posted August 13, 2024. The copyright holder for this preprint (which was not certified by peer review) is the author/funder, who has granted bioRxiv a license to display the preprint in perpetuity. It is made available under aCC-BY-NC-ND 4.0 International license.

amplicons run on a 1% agarose gel before extracting with the Qiagen Gel Extraction Kit (Qiagen, 28704).

Whole Mount Immunostaining of Zebrafish Embryos

Embryos were dechorinated before fixation in 4% paraformaldehyde (PFA) – phosphate buffered saline (PBS) for 2-4 hours at room temperature (or overnight at 4°C) and washed in 0.1% Tween-PBS (PBST). Those embryos used for in situ hybridisation were transferred to 100% methanol and stored at -20°C, while those used for immunostaining were kept in PBST at 4°C until staining.

Embryos in PBST were washed twice in PBS for 10 minutes before permeabilization in 0.25% Trypsin-PBS: 24hpf, 10 min; 48hpf, 12 min; 72hpf, 16 min; 96hpf, 18 min; 120hpf 22 min. The reaction was inhibited by addition of heat inactivated goat serum (HINGS) and embryos were washed three times in PBST for 5 minutes. Blocking was carried out by incubating embryos in 10% HINGS - 0.8% Triton-PBS at room temperature for 4 hours. Primary antibodies were incubated with samples in 2% HINGS – 0.8% Triton PBS at 4°C overnight; the following day embryos were washed several times over the course of 4-6 hours before incubating with the secondary antibody at 4°C overnight. Embryos were washed in 0.8% Triton PBS for several hours before fixation in 4% PFA for 1 hour at room temperature; after washing twice in 0.8% Triton PBS embryos were transferred to 70% glycerol for long-term storage and imaging.

Table 2: Details of antibodies used in wholemount immunostaining of zebrafish larvae.

Antibody	Company	Host Species	Dilution
Anti-FOXG1 (C-terminal)	Abcam, ab196868	Rabbit	1:500
Anti-COX-IV	Abcam, ab33985	Mouse	1:500
Anti-MRPS34	Thermofisher, PA5-59872	Mouse	1:500
Anti-Rabbit Alexa Fluor 488	Abcam, ab150077	Goat	1:1000
Anti-mouse Alexa Fluor 568	Abcam, ab175473	Goat	1:1000

Expansion Microscopy

Immunostaining was performed as previously described before embryo heads were dissected and stored individually in PBS in PCR tubes to allow for genotyping of the tails (performed as detailed above). Following successful genotyping, dissected heads were moved to 1.5ml Eppendorf tubes containing 0.1mg/ml Acrylolyl-X SE in 0.1X PBS with one tube for multiple heads of each genotype. Expansion microscopy was then performed as previously described(*32*).

Quantification of Phenotypic Measurements

bioRxiv preprint doi: https://doi.org/10.1101/2024.08.13.607559; this version posted August 13, 2024. The copyright holder for this preprint (which was not certified by peer review) is the author/funder, who has granted bioRxiv a license to display the preprint in perpetuity. It is made available under aCC-BY-NC-ND 4.0 International license.

To ensure a fair comparison, all embryos that were to be compared were imaged with the same laser power and gain using a Zeiss Axio Imager.Z2 LSM 800 Confocal.

Cell counts of Dlx^+ inhibitory interneurons and $Tbr2^+$ excitatory neurons were performed manually on confocal Z-stacks while blinded. Either the Tbr2 or Dlx channel was combined with DAPI and the counter feature on Fiji was used to mark individual cells while scrolling back and forward through the Z-stack, ensuring no cell was counted twice. Figure 1 shows an example slice with the Tbr2 channel merged with DAPI and cells counted.

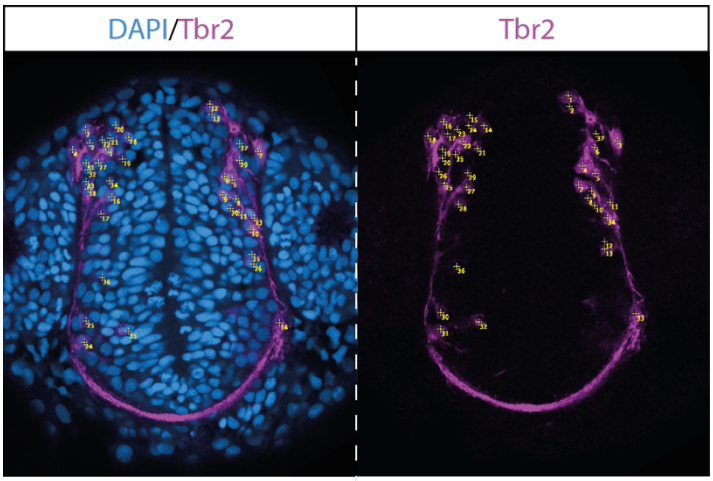

Figure 1: Example of Tbr2 cell counting in a 28hpf embryo. Either Tbr2 (shown) or Dlx channel was combined with DAPI and cells counted with the counting feature in Fiji by scrolling back and forward through a Z-stack.

Quantification of anterior commissure phenotype was also carried out manually while blinded and three measures were used to quantify the anterior commissure phenotype: thickness, width, and volume. A schematic indicating how these measurements were taken can be seen in figure 2.

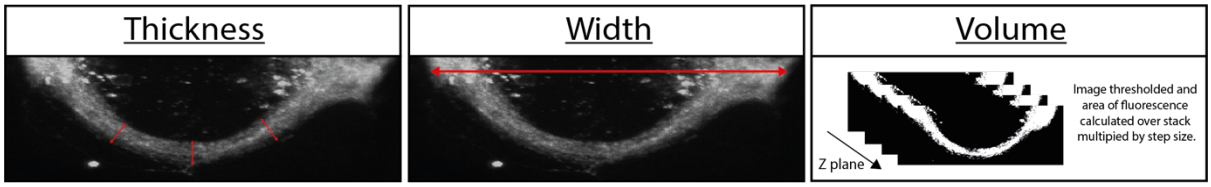

Figure 2: Phenotype measures used in the quantification of anterior commissure (AC) phenotypes. The thickness of the AC was measured in three locations (indicated in figure) following which an average value was calculated for each sample. Width was defined as the length from each lateral edge of the AC. Volume was measured by calculating the area of the AC across the entire 3D-projected image and multiplying by the step size.

To examine differences in Foxg1 protein expression in all cells of the telencephalon the “Analyse Particles” function of Fiji was used; first segmenting Foxg1 expressing cells as regions of interest (ROI) across an entire Z-stack, then measuring the individual fluorescence intensity for each ROI. When characterising cell type specific differences in Foxg1 expression mean fluorescence intensity was calculated for each individual cell type (progenitor, mid, and differentiated) by manually drawing a region

bioRxiv preprint doi: https://doi.org/10.1101/2024.08.13.607559; this version posted August 13, 2024. The copyright holder for this preprint (which was not certified by peer review) is the author/funder, who has granted bioRxiv a license to display the preprint in perpetuity. It is made available under aCC-BY-NC-ND 4.0 International license.

of interest around each cell; the subtype was estimated based on the distance from the ventricle. A schematic showing the selection of different subtypes can be seen in figure 3; for each embryo the maximum number of cells that could fairly be discriminated was counted from two non-overlapping slices in a stack, to ensure the same cell was not included twice.

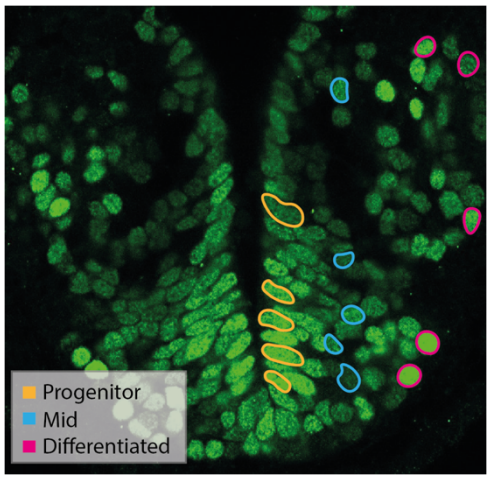

Figure 3: Selection of cells for cell type specific measurements of Foxg1 expression at 2dpf. Cell identity was determined based on location relative to the ventricular wall. Progenitors were situated directly adjacent to the wall (yellow); migrating/differentiating cells (referred to as "Mid") were assigned to those cells between the progenitor population and the cells at the most lateral edges of the telencephalon; postmitotic neurons ("Differentiated") were assigned to those at the lateral-most edges of the telencephalon.

Colocalisation analysis was carried out using the Fiji plugin, "Just another Colocalisation Plugin" (JaCOP,), on Otsu thresholded confocal images (*33*). Alternatively, colocalisation was determined by calculating the percentage of Foxg1 overlapping other stainings. Total Foxg1 area was calculated by Otsu thresholding of the raw image, maintaining the same values for each embryo and subsequent thresholding of non-nuclear Foxg1 images. The DAPI channel was used to produce a ROI and removal of this from the original Foxg1 image determined the non-nuclear Foxg1 staining. Thresholding of the COX-IV or Mrps34 channel was performed with the Otsu method to produce a second ROI and the "clear outside" function in Fiji was used to remove any Foxg1 signal outside of this ROI. Measuring this area allowed for the calculation of non-nuclear Foxg1 overlapping with COX-IV/Mrps34, while removing this ROI from the original Foxg1 image gave the percentage of total Foxg1 overlapping with these markers. The structural mitochondrial phenotype was assessed by use of the Fiji plugin "mitochondrial network analysis tool" (MiNA)(*34*). For each embryo two slices from a z stack were analysed at equivalent anterior and posterior levels between samples.

RNA-sequencing

Single embryos from a *foxg1a*$^{+/-}$ in-cross were dechorinated at the appropriate timepoint (8-somite stage or 24 hours). Embryos were homogenised in buffer RLT from the RNeasy Micro Kit (Qiagen*, 74004*) using a plastic pestle, and RNA extraction was performed as per the manufacturer's instructions, with the inclusion of the optional on-column DNase digestion. The concentration of RNA was determined using the Quibit™ RNA High Sensitivity Assay (Thermofisher*, Q32852*) and the quality

bioRxiv preprint doi: https://doi.org/10.1101/2024.08.13.607559; this version posted August 13, 2024. The copyright holder for this preprint (which was not certified by peer review) is the author/funder, who has granted bioRxiv a license to display the preprint in perpetuity. It is made available under aCC-BY-NC-ND 4.0 International license.

determined by sending an aliquot to the Bioanalyzer facility at King's Genomic Centre, Waterloo Campus. RNA samples with an RNA integrity number (RIN) of less than 8 were discarded and those with the highest RNA concentrations were sent to the genomics facility at the Huntsman Cancer Institute High-Throughput Genomics Facility, University of Utah, USA. Library preparation was carried out using the Illumina TruSeq Total RNA Library Prep Ribo-Zero Gold kit which included depletion of ribosomal RNA prior to cDNA synthesis. Libraries were then sequenced by application to a Illumina NovaSeq flow cell on a NovaSeq 6000 instrument; each sample was read with 2x 50bp paired-end sequencing, with an average of 30 million reads per sample.

All bioinformatics was carried out by Fursham Hamid, a Postdoctoral researcher in the lab at the time of these experiments. In brief, resulting FASTQ files from the RNA-seq experiment were subjected to initial quality control steps before aligning to the Genome Reference Consortium Zebrafish build 10 genome, (GRCz10), with 70-80% of reads aligning to the reference genome. Differential gene expression analysis was performed using Whippet and an excel file containing gene names, log fold changes, and corrected significance values for each genotype were supplied to me along with BAM files. I was then able to characterise changes in gene expression using log fold changes and manual inspection of sequencing reads in IGV to determine which genes may be promising candidates for further investigation. RNA-sequencing data is available online at ArrayExpress under the accession number E-MTAB-13886.

Whole Mount In Situ Hybridisation

A whole embryo cDNA library was produced for use as a template for in situ probe PCR by extraction of RNA from 24 hpf embryos using the Qiagen RNeasy Mini Kit (*Qiagen,* 74104), with inclusion of the optional on-column DNase digest. RNA was reverse transcribed using the First Strand cDNA Synthesis kit (*Thermo Scientific*, K1612), starting with 1µg of RNA and using Oligo(dt) primers. The concentration of resulting cDNA was measured using a nanodrop and diluted to 50ng/µl for use as a template in the production of gene-specific anti-sense RNA probes. Gene-specific mRNA primers were designed using ensemble sequences, with the reverse primer modified to contain a T3 RNA polymerase promoter sequence that would allow the transcription of an anti-sense RNA probe (primers can be seen in table x). PCR reactions for amplification of the gene-specific cDNA templates comprised 50ng of total cDNA, a final concentration of 0.5µM of each of the forward and reverse primers, and 12.5µl Dream Taq Green PCR Master Mix 2X (*Thermo Scientific*, K1081) in a total reaction volume of 25µl; cycling conditions can be seen in table 3.

Table 3: Gene-specific primers for production of *in situ* hybridisation probes. Red indicates the T3 RNA polymerase site for *in vitro* transcription.

Gene	Forward primer	Reverse Primer
e2f7	GGCTCCCACAGACTCTACAG	AGAGCGGCAATTAACCCTCACTAAAGGGTGGAGGCACCGTCAGAAATG
otpb	TTAACGGAGTCACGGGTTCAG	AGAGCGGCAATTAACCCTCACTAAAGGGCCATCATCCAGTAAGGCTGC

Following amplification, gene-specific PCR products were purified with the MinElute PCR Purification kit (Qiagen, 28004) and 500ng was subsequently used in an in vitro

bioRxiv preprint doi: https://doi.org/10.1101/2024.08.13.607559; this version posted August 13, 2024. The copyright holder for this preprint (which was not certified by peer review) is the author/funder, who has granted bioRxiv a license to display the preprint in perpetuity. It is made available under aCC-BY-NC-ND 4.0 International license.

transcription reaction. In a total volume of 20µl, 2µl of digoxgenin-labelled (DIG) NTPs (*Roche,* 11277073910), 2µl 10X transcription buffer (*Roche*), 1µl Pyrophopatase (Thermo Scientific, EF0221), 1µl RNase Inhibitor (*Roche,* 10877200), and 1.5µl of T3 RNA polymerase (*Roch,* 11031163001) were added to PCR templates and incubated at 37oC for 1 hour, 1.5µl of DNase was then added and reaction incubated for a further 15 minutes.

DIG labelled RNA probes were then purified using Mini Quick Spin Columns (*Roche,* 11814427001) before addition of 1 volume of saline-sodium citrate (SCC) and 2 volumes of formamide to the total RNA.

Embryos collected as previously described were rehydrated from 100% methanol to PBST gradually, at room temperature, before permeabilising for 10 – 30 minutes with Proteinase K in PBST (1:1000 dilution). After washing twice in PBST, embryos were fixed in 4% PFA for 20 minutes at room temperature and washed again in PBST. 100µl Hybridisation mix (*10% TWEEN, 50% formamide, 5X SCC, 0.5mg/ml Torula mRNA, 0.05mg/ml heparin*) heated to 65^{o}C was added to the embryos, shaking at room temperature until they settled; embryos were moved to 65^{o}C and Hybridisation mix replaced before incubating for 3-6 hours. Anti-sense RNA probes were diluted accordingly in pre-warmed Hybridisation mix, applied to the embryos and hybridised overnight at 65^{o}C.

Embryos were washed in 65^{o}C Hyb mix for 30mins, in 2X SSE (*3M Sodium chloride, 0.3M sodium citrate, pH 7*) 0.1% CHAPS multiple times over 1.5 hours and then several times in 0.2X SSE 0.1% CHAPS over 1.5 hours before washing in 0.1% TWEEN Maleic acid buffer (MABT) for 1 hour. Blocking was performed in MAB/blocking buffer for 2 hours before adding MAB/Anti-DIG (1:2000) AP Fab fragments (*Roche*, 11093274910) and incubating overnight at 4^{o}C. Embryos were washed over the course of 6 hours in MABT followed by multiple washes in TBST, leaving overnight at 4^{o}C.

Embryos were washed twice in NTMT (*0.1M NaCl, 0.1M Tris-HCl, 0.05M MgCl, 0.1% TWEEN*) pH9 for 5 minutes before incubation in 3.375µl NBT (*Roche,* 11383213001) and 3.5µl BCIP (*Roche,* 1183221001) per 1.5ml NTMT. Staining was monitored and colouration ended when reaching the desired intensity before washing several times in PBST. Following a final fixation step in 4% PFA for 1 hour at RT embryos were washed in PBST and stored in 70% glycerol until imaging, using a Nikon eclipse E800 microscope.

Wholemount RNA Hybridisation Chain Reaction (HCR)

HCR was performed as described in Ibarra-García-Padilla *et al.*, (2021), followed by immunostaining as described previously in this manuscript, omitting permeabilization with trypsin and using PBS-0.1% TWEEN.

Protein Extraction from Zebrafish Embryos

bioRxiv preprint doi: https://doi.org/10.1101/2024.08.13.607559; this version posted August 13, 2024. The copyright holder for this preprint (which was not certified by peer review) is the author/funder, who has granted bioRxiv a license to display the preprint in perpetuity. It is made available under aCC-BY-NC-ND 4.0 International license.

Protein for Western Blot experiments was extracted from 24hpf zebrafish embryos obtained from an in cross of *foxg1a*$^{+/-}$*, Dlx4-6;GFP* adults. Use of the Dlx transgenic background enabled genotyping of embryos by eye under epifluorescence microscopy: *foxg1a*$^{5bp/5bp}$ fish exhibit an obvious lack of Dlx+ interneurons in the telencephalon and *foxg1a*$^{+/5bp}$ have a significant decrease that is visible to the trained eye. Previous validation of this genotyping method gave a 95% success rate for validating heterozygous mutants, while homozygous mutants were always correctly identified.

Yolks were removed from dechorinated embryos by washing them twice in Ringer's Solution (*116mM NaCl, 2.9mM KCl, 1.8mM* $CaCl_2$*, 5mM HEPES pH 7.2*), before adding Ringer's solution complete with Protease Inhibitor Cocktail (*Roche, 11836170001*) and tirating with a pulled glass pipette. Next, embryos were centrifuged for 3 minutes at 1000g and the supernatant removed, fresh Ringer's solution (without Protease Inhibitor Cocktail) was added to the samples and the centrifugation carried out again; this wash step was repeated three times. NP40 buffer, complete with Protease Inhibitor Cocktail (*Roche,* 11836170001), was added to the samples and incubated on ice for 10 minutes before homogenising with a sterile syringe. Samples were then centrifuged at 4^{o}C at maximum speed for minutes to remove the insoluble cellular material, with the supernatant formed after this step being transferred to a new Eppendorf.

Protein concentration was quantified using the Pierce™ BCA Protein Assay (*Thermofisher,* 23225), as per the manufacturer's instructions. Protein samples were then either directly used in SDS page or stored at -80^{o}C until needed.

Immunoprecipitation (IP)

IP was performed with the Pierce™ Crosslink IP (*Thermofisher, 26147*) kit using total protein lysate extracted at 24hpf as previously described. Antibodies were bound to agarose resin as detailed in the user manual by incubating with rotation at 4^{o}C overnight prior to crosslinking with DSS (included in kit) for 45mins at RT. Pre-clearing of total lysate was performed as indicated using 1mg of total lysate for each IP (*Mrps34; PA5-59872, IgG; 02-6102, and Foxg1; ab196868*). Captured peptides were eluted with low pH buffer before denaturation at 95^{o}C for 10mins.

Zebrafish Western Blot

Protein lysate was diluted in NuPAGE™ LDS Sample Buffer (*Thermofisher,* NP0007) and heated to 70^{o}C for 10 minutes. 15µg of total protein lysate was run per well of a NuPAGE™ 10% Bis-Tris Mini Protein Gel (*Thermofisher,* NW00105BOX), alongside a Dual Precision Protein Standard (*BioRad,* 1610374), for 1 hour at 100V. Protein was then transferred to a membrane using the iBlot2 machine, with iBlot2 PVDF Regular Stacks (*Thermofisher,* 1B24001), and template programme P0 (20V, 1 minute; 23V 4 minutes; 25V 2 minutes). The blot membrane was then blocked in 5% Milk – TBST for 45 minutes at room temperature. After blocking, primary antibodies were added in 2% Milk – TBST overnight at 4^{o}C while shaking (*Rabbit anti-C-terminal FOXG1* ab196868*, 1:500; Rabbit anti-N-terminal FOXG1* PAB30085*, 1:500; Rabbit anti-GAPDH, 1:500*).

bioRxiv preprint doi: https://doi.org/10.1101/2024.08.13.607559; this version posted August 13, 2024. The copyright holder for this preprint (which was not certified by peer review) is the author/funder, who has granted bioRxiv a license to display the preprint in perpetuity. It is made available under aCC-BY-NC-ND 4.0 International license.

The following day the blot membrane was washed 3 times in TBST, before adding the secondary antibody, goat anti-rabbit IgG HRP (*Abcam,* ab6721) in 2% Milk-TBST and incubating at room temperature for 1 hour. The membrane was then washed three times with TBST before incubation with Pierce™ ECL Plus Western Blotting Substrate (*Thermofisher,* 32132), as per the manufacturer's instructions. Blot membranes were exposed using LICOR Odyssey XF imaging system.

Quantification of the relative expression of different C-terminal Foxg1 fragments was carried out in Fiji using the "analyse gels" feature. Three separate Western Blot experiments, performed on different biological material, were used to calculate relative expression differences normalising to the housekeeping gene GAPDH as outlined in (*36*)

Cloning and Constructs

All restriction enzyme digests were carried out using the NEB cloner online protocol database (*https://nebcloner.neb.com/#!/).* Following digestion all products were PCR purified with Qiagen's MinElute PCR purification kit (28004) and DNA concentrations measured using a nanodrop instrument. Ligations were performed using the Instant Sticky-end Ligase Master Mix (*NEB*, M0370S), as per the manufacturer's instructions. Molar ratio of ligation mixes ranged from 1:3 – 1:7.

Transformation of cloned vectors was achieved by incubating 2µl of ligation mix, or 10ng of vector, with NEB 5-alpha Competent E.Coli (C2987H) on ice for 30 minutes before heat shock at 42°C for 45 seconds and returning to ice for 2 minutes. Outgrowth was allowed in SOC Medium while shaking at 37°C for 45 minutes before plating on an appropriate antibiotic selective agar plate and incubating at 37°C overnight.

Single colonies were selected, grown overnight in antibiotic selective agar broth, and plasmid purified using Qiagen's MiniPrep Spin Kit (*Qiagen*, 27104). DNA concentration was measured using a nanodrop instrument and vectors sent for sequencing to confirm correct cloning.

QUAS: Syp-GFP

For telencephalic-specific labelling of excitatory synapses, a 5' UAS: Synaptophysin-GFP vector (gift from Meyer lab) was modified to include a QUAS binding sequence instead of the classic Gal4;UAS system. This allowed for microinjection of the QUAS: Syp-GFP construct into our Foxg1 TALEN x Tg(tbr2:QF2)c714;Tg(QUAS:mApple-caax:HE:mCherry) zebrafish line, resulting in the labelling of only excitatory synapses. The UAS sequence from the original vector was excised by PciI (*NEB*, R0655S) and HindIII (*NEB*, R0104S) restriction enzyme double digest. Primers were designed against the QUAS sequence in the transgene of Tg(tbr2:QF2)c714;Tg(QUAS:mApple-caax:HE:mCherry), including a PciI restriction digest site in the forward primer (5'-TTGCTCACATGTCAACTTTGTATAGAAAAGTTGG-3') and a HindIII site in the reverse (5'-AGCAAAAAGCTTCTTTTTTGTACAAACTTGACGC-3'). Genomic DNA from was extracted as previously described and a 230bp product was amplified using

bioRxiv preprint doi: https://doi.org/10.1101/2024.08.13.607559; this version posted August 13, 2024. The copyright holder for this preprint (which was not certified by peer review) is the author/funder, who has granted bioRxiv a license to display the preprint in perpetuity. It is made available under aCC-BY-NC-ND 4.0 International license.

the DreamTaq Green PCR Mastermix (*Thermofisher*, K1081). The PCR product was then PCR purified with Qiagen's MinElute PCR purification kit (28004) and digested with PciI and HindIII. The cut vector and the digested PCR product were then re-purified, ligated and transformed as described above.

Following conformation of cloning success by Sanger sequencing, 60pg of QUAS:Syp-GFP was injected into Tg(tbr2:QF2)c714;Tg(QUAS:mApple-caax:HE:mCherry) in the *foxg1a* background. Embryos were then fixed and imaged as previously described and the Fiji plugin, "SynQuant" was used to characterise synaptic phenotypes. The SynQuant plugin allowed for automated detection of synaptic puncta based on QUAS:Syp-GFP images; an example of puncta detection can be seen in figure 4(*37*).

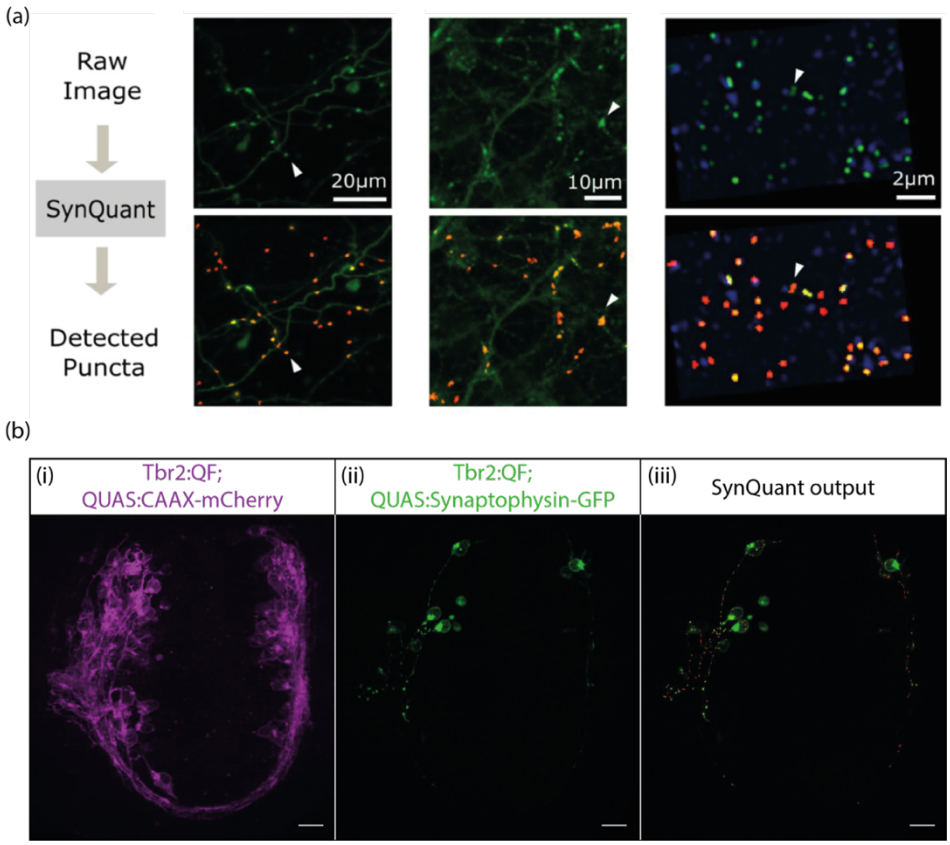

Figure 4: Automatic detection of synaptic puncta using SynQuant. (a) Examples of input images and the resultant detected synaptic puncta from Wang et al, 2020. **(b)** Representative images from labelling of excitatory synapses in *foxg1a* mutants using SynQuant. **(i)** Confocal projection of Tbr2+ cell membrane labelling in our transgenic line. **(ii)** Example of labelling achieved upon injection of QUAS:Synaptophysin-GFP construct, showing that labelling colocalises only with Tbr2+ cells. **(iii)** Representative SynQuant output for the automatic detection of synaptic puncta on QUAS:Synaptophysin-GFP images.

Morpholino Design Against Cryptic ATGs

The size of the truncated protein present in the *foxg1a* homozygous and heterozygous mutants was determined using Western Blot; the size in bp was then determined using a kDa to bp calculator and the *foxg1a* gene was inspected for potential cryptic start sites. Two ATGs were identified that could produce a protein of ~35kDa (figure 5), since they were in direct sequence with each other one MO was designed to target

bioRxiv preprint doi: https://doi.org/10.1101/2024.08.13.607559; this version posted August 13, 2024. The copyright holder for this preprint (which was not certified by peer review) is the author/funder, who has granted bioRxiv a license to display the preprint in perpetuity. It is made available under aCC-BY-NC-ND 4.0 International license.

them both. From this point on these ATGs are denoted ATG_4 & ATG_5; this nomenclature was determined by counting the in-frame ATGs along the *foxg1a* gene. MOs were designed by Gene Tools Inc using submitted sequences with the target ATG highlighted: MO sequence against ATG_4 & ATG_5: GGCCATCATAATCAAAGCGTTGTAG. The MO was diluted to 0.6mM and 1nl injected into 1-cell stage embryos, before either extracting protein for Western Blot or fixation for antibody staining.

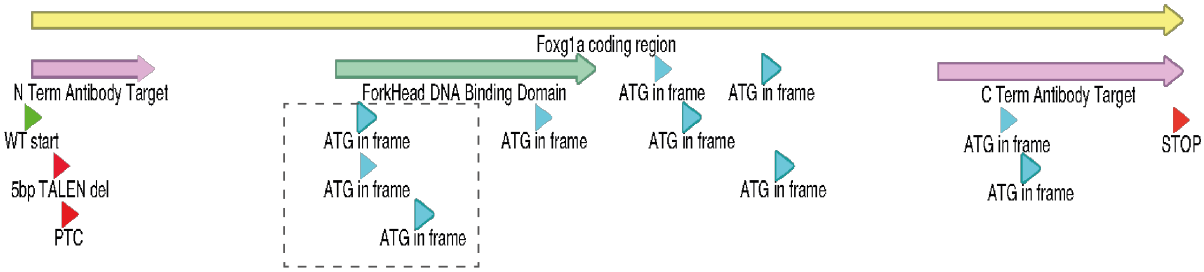

Figure 5: Schematic of the *foxg1a* coding region. The position of the 5bp TALEN deletion and subsequent premature termination codon (PTC) are indicated in red. Downstream in-frame ATGs are indicated in blue, with the three potential cryptic start codons (CSCs) in use highlighted by a dashed box.

Mitochondrial Stress Test of 48hpf Zebrafish Larvae

Embryos from a *foxg1a*$^{+/5bp}$ incross were injected with 1nl of 0.6mM of either a control MO or the MO against ATG4&5. Embryos were dechorinated at 24hpf and maintained at 28^{o}C in pH 7.4 E3 media until they reached 48hpf. The Seahorse flux cartridge (*103792-100, Agilent)* was rehydrated with 200µl of sterile water per well overnight at 37^{o}C and the Seahorse XF machine was calibrated to room temperature. Drug stocks were prepared in pH7.4 E3 media such that the final concentration upon injection of 20µl per well was as follows: Oligomycin; 25µm (*495455-10MG, Sigma*), FCCP; 8µm (*C2920-10MG, Sigma*), Antimycin A; 1.5µm (*A8674-50MG, Sigma*), and Rotenone; 1.5µm (*R8875-10MG, Sigma*). Following overnight rehydration, the sterile water was removed from the Seahorse cartridge and replaced with 200µl per well of calibrant solution pre-warmed to 37^{o}C (*100840-000, Agilent*). For each well 20µl of prepared drug solution was loaded into the corresponding injection port (Oligomycin; A, FCCP; B, Antimycin A and Rotenone; C). The sensor cartridge was then loaded into the machine and calibration commenced. Embryos for the Mitochondrial Stress Test were moved to a new dish containing pH7.4 E3 media supplemented with MS222 and a P1000 pipette set to 180µl was used to transfer individual larvae to each well of the test cartridge, leaving the four corner wells devoid of fish to allow for background readings. After calibration was completed the first cartridge was removed and replaced with the cartridge containing anesthetised larvae before beginning the Mitochondrial Stress Test Cycling, as detailed in table 4. Following completion of the procedure, individual larvae were genotyped as previously described and data was analysed using the online Wave software from Agilent.

bioRxiv preprint doi: https://doi.org/10.1101/2024.08.13.607559; this version posted August 13, 2024. The copyright holder for this preprint (which was not certified by peer review) is the author/funder, who has granted bioRxiv a license to display the preprint in perpetuity. It is made available under aCC-BY-NC-ND 4.0 International license.

Table 4: Cycling conditions for Seahorse Mitochondrial Stress Test

	mix	wait	measure	cycles
Baseline	2	1	2	12
Oligomycin	2	1	2	20
FCCP	2	1	2	8
Rotenone/AA	2	1	2	12

Cell Culture

iPSC Culture

Isogenic iPSC lines were produced by Graham Cocks of the King's College London Genome editing core facility and obtained as liquid nitrogen frozen stocks. Alternatively, FOXG1 Syndrome patient iPSCs containing a *FOXG1 256DupC*$^{+/-}$ mutation were obtained from Angus Clarke at Cardiff University as frozen stocks. Cell lines were rapidly thawed and resuspended in StemFlex™ media (*Thermofisher, A3349401*), supplemented with 10µm ROCK inhibitor. Cells were plated on Nunc™ treated 6-well cell culture plates (*Thermofisher, 140685*) previously coated in Geltrex™ (*Thermofisher, A1413301*), as per the manufacturer's instructions. After 24 hours media was replaced with StemFlex™ media without ROCK inhibitor, following which, media was replaced every 2 days. iPSCs were cultured until 70-80% confluency before passaging at a ratio of 1:6: cells were washed with room temperature (RT) Hanks Balanced Salt Solution (HBSS; *Thermofisher; 14170088*) and dissociated by adding 1ml Versene (*Thermofisher, 12569069*) incubated for 3-5mins at 37°C. Versene was aspirated from the culture vessel and StemFlex™ media was used to collect the cells gently with a cell scraper. Frozen cell stocks were prepared by dissociating cells as described and resuspending iPSCs from a single well of a 6-well plate in 1ml of StemFlex™ 10% DMSO (*Sigma, D2650*). Cells were cooled to -80°C at a rate of -1°C per min using a Mr Frosty container (*Thermofisher, 5100-0001*), after 24 hours cells were transferred on dry ice to liquid nitrogen for long term storage.

Neuralisation

iPSCs for neural induction were cultured on Geltrex coated plates until 100% confluent to ensure generation of CNS-specific neuronal precursor cells (NPCs). When confluency was reached StemFlex™ media was aspirated, and Neuralisation media (components in table 5) was added to the cells - the addition of neuralisation media was denoted as day 1 in the neuralisation timeline. Addition of Dorsomorphin and SB43 to culture media allowed for neural induction via dual SMAD inhibition: SB43 acting on activin/nodal/TGF-β and Dorsomorphin inhibiting both activin/nodal/TGF-β and BMP pathways (*38*).

Table 5: Components of neuralisation media for dual SMAD inhibition protocol.

bioRxiv preprint doi: https://doi.org/10.1101/2024.08.13.607559; this version posted August 13, 2024. The copyright holder for this preprint (which was not certified by peer review) is the author/funder, who has granted bioRxiv a license to display the preprint in perpetuity. It is made available under aCC-BY-NC-ND 4.0 International license.

Media	Component
N2	49ml DMEM (*Sigma,D6421*), 0.5ml 100x N2 (*Thermofisher, 1750248*), 0.5ml 100X Glutamax (*Thermofisher, 35050-061*)
B27	48.5ml Neurobasal (*Thermofisher, 21103049*), 1ml 50X B27 (*Thermofisher, 17504044*), 0.5ml 100X Glutamax (*Thermofisher, 35050-061*)
Neuralisation Media (N2B27)	50% N2, 50% B27, 1µM dorsomorphin (*Sigma, P5449-5MG*), 10µM SB43 (*Sigma, S4317-5MG*)

Neuralisation media was replaced every 24 hours until day 8, when NPCs were passaged at a ratio of 1:1. After aspiration of media, cells were washed in RT HBSS before the addition of 1ml Accutase (*Sigma, A6964-500ML*) for each well of a 6-well plate. NPCs were incubated at 37°C for 3-5mins until able to be lifted from the vessel with gentle pipetting, cells were transferred to a falcon tube containing RT DMEM and centrifuged for 2 mins at 900RPM. The supernatant was aspirated, cells resuspended in RT DMEM and centrifuged for a further 2 mins to ensure all Accutase had been eliminated. NPCs were then resuspended in Neuralisation media without the addition of Dorsomorphin and SB43, supplemented with 10µm ROCK inhibitor to promote cell survival and plated on Geltrex coated plates. Media was replaced every day until day 13, when cells were once again passaged at a ratio of 1:1; on day 16 and 23 cells were passaged as described, but at a ratio of 1:2.

For terminal differentiation of neurons, coverslips were coated with Poly-D-Lysine (*A3890401, Thermofisher*) diluted to 50µg/ml in Borate buffer (*28341, Thermofisher*) and incubated at 37°C for at least 4 hours. Coverslips were then washed three times with PBS before replacing with laminin (*Merck, L2020-1MG*) diluted to 9.6µg/ml in cold DMEM and incubated overnight at 37°C. NPCs for terminal differentiation were passaged with Accutase, as previously described, and plated on laminin coated coverslips at a density of 200,000 cells/cm^2 in B27 media supplemented with 10μM DAPT (*Stem Cell Technologies, 72082*), 200μM AA2P (*Merck, A4403*), and 10μM ROCKi. Following 24 hours of incubation the total volume of media was removed and replaced with B27 supplemented with DAPT and AA2P; media was replaced every day for 7 days following terminal plating. Following this, a part media change was performed every 7 days omitting DAPT from the media. Coverslips for immunocytochemistry were fixed in 4% PFA for 10 mins at RT before permeabilization in 2% HINGS 0.4% TRITON-PBS for 30 mins. Primary antibodies added in 2% HINGS 0.4% TRITON-PBS and incubated overnight at 4oC before washing 3X in 0.4% TRITON-PBS, secondary antibodies were incubated for 1 hour at RT in 2% HINGS 0.4% TRITON-PBS and samples washed 3X before mounting. Details of antibodies for ICC can be found in table 6.

Table 6: Antibodies used in human ICC.

bioRxiv preprint doi: https://doi.org/10.1101/2024.08.13.607559; this version posted August 13, 2024. The copyright holder for this preprint (which was not certified by peer review) is the author/funder, who has granted bioRxiv a license to display the preprint in perpetuity. It is made available under aCC-BY-NC-ND 4.0 International license.

Antibody	Company	Host Species	Dilution
Anti-FOXG1 (C-terminal)	Abcam, ab196868	Rabbit	1:100
Anti-COX-IV	Sigma, T6793	Mouse	1:100
Anti-MRPS34	Thermofisher, PA5-59872	Mouse	1:100
Anti-NeuN	Abcam, ab104224	Mouse	1:100
Anti-Tbr1	Abcam, ab183032	Rabbit	1:100
Anti-Rabbit Alexa Fluor 488	Abcam, ab150077	Goat	1:1000
Anti-mouse Alexa Fluor 568	Abcam, ab175473	Goat	1:1000